Applications in Energy and Combustion Science 1–4 (2020) 100008

Contents lists available at ScienceDirect

Applications in Energy and Combustion Science

journal homepage: www.elsevier.com/locate/jaecs

A review of laminar flame speeds of hydrogen and syngas measured from propagating spherical flames

Wang Han [a], Peng Dai [b], Xiaolong Gou [c], Zheng Chen [d,*]

[a] Institute for Multiscale Thermofluids, School of Engineering, The University of Edinburgh, Edinburgh EH8 3JL, Scotland, UK
[b] Department of Mechanics and Aerospace Engineering, Southern University of Science and Technology, Shenzhen 518055, China
[c] Key Laboratory of Low-grade Energy Utilization Technologies and Systems, School of Power Engineering, Chongqing University, Chongqing 400044, China
[d] SKLTCS, CAPT, BIC-ESAT, College of Engineering, Peking University, Beijing 100871, China

ARTICLE INFO

Keywords:
Laminar flame speed
Propagating spherical flame
Hydrogen
Syngas
Uncertainty

ABSTRACT

As promising alternatives to fossil fuels, hydrogen (H_2) and syngas are playing important roles in the development and control of high-efficiency, low-emission engines. Achieving accurate prediction of H_2-fueled combustion requires a reliable chemical mechanism which, however, still exists considerable uncertainty. The laminar flame speed (LFS) has been widely employed to validate and optimize chemical mechanisms and to model turbulent premixed combustion. While in the literature there are extensive LFS data measured using the outwardly propagating spherical flame (OPF) method for hydrogen/air and syngas/air mixtures at normal temperature and pressure (NTP), the accuracy of the LFS data is not fully explored. This work aims to (i) review the uncertainty in the LFSs measured by different groups for hydrogen/air and syngas/air mixtures at NTP using the OPF method, and (ii) identify underlying sources of the uncertainty. It is found that there are considerable discrepancies in the LFS measurements, leading to these experimental data being unreliable for restraining the uncertainty of chemical models. The underlying sources of uncertainty are discussed in different flame propagation regimes and their contributions to the discrepancies are assessed individually using 1-D simulations. The results show that the contribution of ignition effects to the uncertainty depends strongly on the equivalence ratio and that the ignition effects could be one of the main sources of uncertainty for the LFSs of fuel-rich mixtures. Furthermore, it is found that the accuracy of measured LFSs is strongly affected by the choice of extrapolation model and flame radius range for extrapolation. The nonlinear extrapolation is less sensitive to the flame radius range than linear extrapolation, implying that using nonlinear extrapolation models can reduce the impact of the flame radius range selected on the uncertainty, especially for fuel-rich and/or fuel-lean mixtures. Nevertheless, strong nonlinear behavior between stretched flame speed and stretch rate still makes a major contribution to the very large discrepancies even when the nonlinear extrapolation models are used. To address the nonlinear stretch behavior, a new nonlinear extrapolation model NQH is proposed and it is shown to be more accurate than other models as pressure increases. Moreover, the recommendations on H_2 and syngas LFS measurements using the OPF method are provided.

1. Introduction

As renewable fuels, hydrogen (H_2) and syngas (H_2/CO) are promising alternatives to traditional fossil fuels [1]and play an increasingly important role in the development and control of high-efficiency, low-emission power and propulsion systems. Owing to the recent significant progress in H_2 generation, storage and transportation, the two renewable fuels are becoming cleaner to produce and hence more readily available for use. For instance, the strategy of hydrogen addition has been investigated and employed in internal combustion [2–7] and gas turbine [1,8,9] engines due to the rapid consumption of fossil fuels and increasingly stringent emission standards. Moreover, hydrogen-rich syngas can be used in advanced gas turbine engines to achieve high efficiency and low emission [1,10]. In this sense, a fundamental understanding of hydrogen and syngas combustion would help to develop clean power and propulsion systems. Besides, the oxidation mechanisms for hydrogen and syngas are basic building blocks required in developing chemical mechanisms for large hydrocarbon fuels. Therefore, in the literature there are extensive studies on the fundamental combustion properties of hydrogen and syngas (e.g. [1,11–14]). In this study we focus on the **L**aminar **F**lame **S**peed (LFS) of hydrogen/air and syngas/air mixtures.

LFS is one of the most important physicochemical properties of a combustible mixture, which is defined as an adiabatic, premixed, un-

* Corresponding author.
E-mail address: cz@pku.edu.cn (Z. Chen).

https://doi.org/10.1016/j.jaecs.2020.100008
Received 9 August 2020; Received in revised form 1 October 2020; Accepted 19 October 2020
Available online 25 October 2020

stretched, and planar flame propagation speed relative to the unburned mixture [15,16]. It is widely used to examine fuel burning rate and to test and validate detailed and/or simplified mechanisms. Moreover, LFS, as one of the most important parameters, is typically considered to develop an understanding of complex combustion phenomena (e.g., flame stabilization, flashback, and extinction) [15,17,18] and to model turbulent premixed combustion [18–20]. In this context, achieving accurate LFS measurements is extremely desired in order to play its appropriate role in the above description. In the previous studies, different flame configurations have been employed to measure the LFS [21], such as counterflow/stagnation flame, Bunsen flame, burner-stablized planar flame, and **O**utwardly **P**ropagating spherical **F**lame (OPF). Compared to other configurations, the OPF method is one of the most promising approaches for LFS measurements because of its simple flame configuration and readily defined stretch rate, especially for measuring LFSs under high pressure conditions where the other methods are typically not accessible. In this work we discuss the LFS measured from the OPF method only.

As reviewed in [22–24], many studies have been conducted to measure the LFSs for hydrogen and syngas. However, as shall be shown in this study, there are large discrepancies in the LFSs measured for hydrogen/air and syngas/air mixtures even at **N**ormal **T**emperature and **P**ressure (NTP, $T_u = 298\,\mathrm{K}$, $P = 1\,\mathrm{atm}$). It is expected that the substantial discrepancies could bring a challenge with respect to employing the LFSs to validate/optimize chemical mechanisms and improve turbulent premixed combustion models. Therefore, great effort needs to be made to improve the accuracy of the LFSs measured by the OPF method. Furthermore, it is necessary to identify the potential sources of uncertainty, which would help to reduce the discrepancies in LFS measurements. Moreover, these uncertainty factors should be considered when using the LFSs data to validate and optimize kinetic models [25,26]. To the authors' knowledge, this work is the first attempt to perform uncertainty quantification and analysis for the LFSs of hydrogen/air and syngas/air mixtures measured by the OPF method with the help of experimental data and simulation results obtained with detailed chemistry and transport models.

With this background, the objective of the present work is twofold: (1) to review the discrepancies in LFSs measured by different groups for hydrogen/air and syngas/air mixtures at NTP using the OPF method; and (2) to identify the underlying factors that could cause/affect the uncertainty in the LFSs by one-dimensional OPF simulations because the numerical OPF method can help to isolate and examine different sources of uncertainty individually, in which a new LFS extrapolation model will be proposed and validated using simulation data at different pressure levels.

The current paper is organized in the following way. First, the OPF method and numerical method are introduced in Section 2; then, the discrepancies in LFSs measured by different groups for hydrogen/air and syngas/air are reviewed in Section 3; the source of uncertainty is discussed in Section 4; and finally, the conclusions and recommendations are presented in Section 5.

2. Experimental and numerical OPF methods

2.1. Experimental OPF method

In the context of OPF measurement methods ([21,27–29] and references therein), a quiescent fuel/air mixture is contained inside a closed chamber. The mixture is centrally ignited by a laser beam or an electrical spark which results in an OPF. The LFS can be measured from the OPF based on two methods i.e. constant-pressure method (e.g. [30–36]) and constant-volume method (e.g. [37–43]). In the constant-pressure OPF method, a closed chamber with optical access is designed, and during the measurement the OPF front history, $R_f = R_f(t)$, can be captured using the high speed Schlieren photograph, shadowgraphy or laser tomography techniques. The LFS is then determined from the flame front history

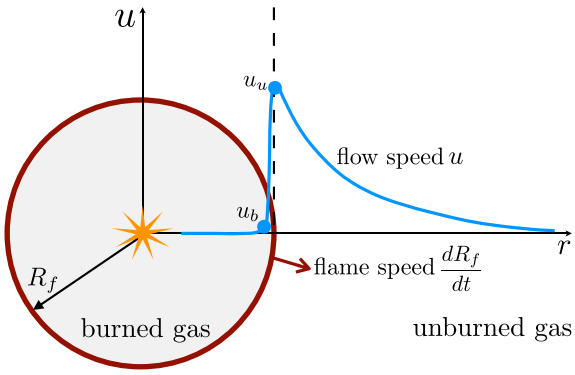

Fig. 1. Schematization of an Outwardly Propagating spherical Flame (OPF), in which the flame front (at $r = R_f$) and the profile of flow speed (u) are indicated in red and blue lines, respectively.

by extrapolating the stretched flame speed (dR_f/dt) to zero stretch rate. On the other hand, a closed thick-walled spherical chamber is used and the chamber pressure history, $P = P(t)$, is recorded by a fast-response pressure transducer in the constant-volume OPF method. The LFS is then determined from the pressure history recorded after the flame has grown to a sufficiently large size such that the pressure rise is evident. It is noted that only a range of the pressure trace can be used where stretch effects and heat losses to the wall are negligible [44]. Furthermore, it should be mentioned that the constant-volume OPF method has the advantage in terms of measuring LFSs over a broad range of initial temperature and pressure from a single test [27]. However, it is challenging to obtain a one-dimensional OPF as cellular instability might develop over the flame surface during its propagation in air, which can greatly affect the accuracy of LFS measurements. Compared to the constant-volume OPF method, the constant-pressure OPF method has the advantage in obtaining more accurate LFSs and thereby it is much more popularly used to measure the LFS. In this context, this study investigates the constant-pressure OPF method only and in this following the OPF method is denoted as the constant-pressure OPF method only.

For an OPF, as shown in Fig. 1, the stretched flame speeds relative to the unburned and burned mixtures are respectively [45]:

$$S_u = \frac{dR_f}{dt} - u_u \tag{1}$$

$$S_b = \frac{dR_f}{dt} - u_b \tag{2}$$

where dR_f/dt is the OPF front propagation speed; u_u and u_b are the flow speeds of unburned and burned gases at the flame front, respectively. Typically, it is difficult to measure the transient flow speed distribution during the spherical flame propagation though the PIV technique has been used by a few groups [46–48]. Moreover, the flow speed of unburned gas varies considerably near the flame front. Therefore, it is challenging to accurately determine S_u from u_u according to Eq. (1) [49].

During the early stage of spherical flame propagation, the increase in pressure is negligible and the burned gas is nearly static, i.e., $u_b = 0$. Consequently, according to Eq. (2) we have $S_b = dR_f/dt$. As a result, the LFS, S_b^0, and the corresponding Markstein length, L_b, can be obtained using the following linear or nonlinear extrapolation models [50–52]:

$$S_b = S_b^0 - L_b \cdot K \tag{3}$$

$$\frac{S_b}{S_b^0} \ln\left(\frac{S_b}{S_b^0}\right) = -L_b \cdot \kappa \tag{4}$$

where $K = \frac{2}{Rf}\frac{dR_f}{dt}$ and $\kappa = \frac{2}{Rf}$ are the stretch rate and curvature of the OPF front, respectively. The LFS, S_u^0, can be computed by $S_u^0 = \sigma S_b^0$, in which σ denotes the density ratio of the burned mixture to the unburned

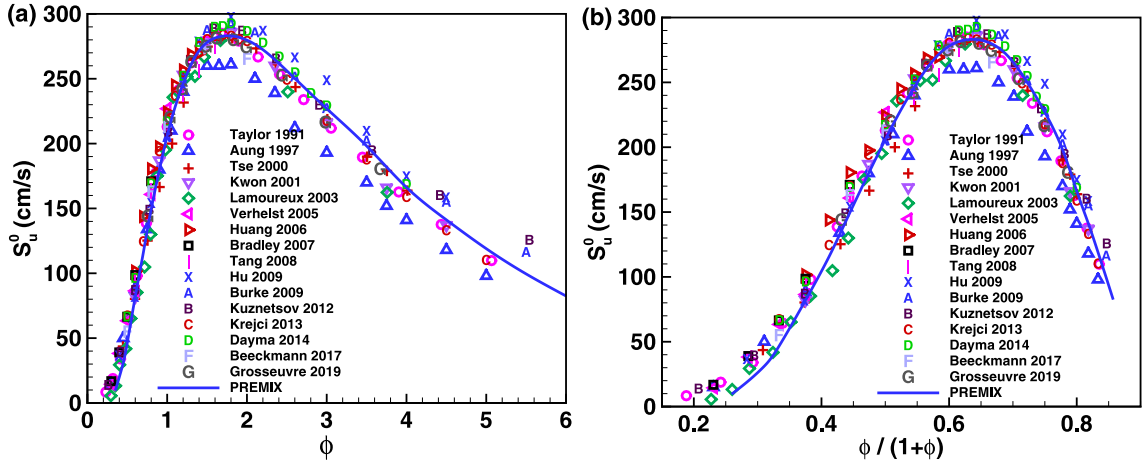

Fig. 2. Laminar flame speed of H_2/air at NTP as a function of equivalence ratio (a) and normalized equivalence ratio (b). The symbols denote experimental results from [80–95]. The line denotes numerical results predicted by the mechanism of Li et al. [73] using CHEMKIN-PREMIX code [105].

mixture at equilibrium condition. Note that the assumption of $u_b = 0$ is only reasonable when radiation effects are negligible and that for slowly propagating flames u_b is not equal to zero, as discussed in Section 4.3.

2.2. Numerical methods

Since the OPF has a simple one-dimensional spherical geometry and there is no complicated interaction between the OPF and the combustion chamber when the pressure rise is negligible, one-dimensional simulations of OPFs can be readily conducted to investigate the performance of the above OPF method. Currently the OPF has been mainly simulated by two in-house codes: A-SURF (**A**daptive **S**imulation of **U**nsteady **R**eactive **F**low) [53–55] and TORC (**T**ransient **O**ne-dimensional **R**eacting flow **C**ode) [56,57]. In order to quantify the uncertainty in LFS measurements, we perform a series of simulations using A-SURF for OPFs in hydrogen/air and syngas/air mixtures over a wide range of equivalence ratios and pressures. More details about the numerical methods used in A-SURF are discussed in [53–55,58–72]. The detailed chemical mechanisms and transport models are included in the simulations of spherical flame propagation in H_2/air and H_2/CO/air mixtures. The mechanisms of Li et al. [73] and Davis et al. [74] are used for H_2/air and H_2/CO/air, respectively. It is noted that the two mechanisms used are optimized for the conditions investigated in this paper. Since previous studies [75–79] showed that Soret diffusion could affect flame propagation in H_2/air and H_2/CO/air mixtures, the Soret effect is included in the A-SURF calculations. In this work, grid convergence is ensured, and a large chamber radius of $R_W = 100\,\text{cm}$ is used in the simulations to suppress confinement effect that will be discussed in Section 4.3.

3. Discrepancies in LFSs measured for hydrogen and syngas

In this section, the LFSs measured for hydrogen/air and syngas/air mixtures at NTP reported in the literature are reviewed, and the discrepancies in the LFSs by different groups using the OPF method are investigated and interpreted. Here we only consider a typical syngas with an equivalent molar of H_2 and CO (i.e. H_2:CO=50%:50% in volume). Table 1 lists the information of initial temperature and pressure, range of equivalence ratio, extrapolation model, range of data used in extrapolation, and geometry of the chamber used by different groups [80–104]. The experimental LFS data and the discrepancies among them will be presented and discussed first in the following. Then, the potential source of uncertainty will be identified and analyzed in Section 4.

Figure 2 shows the LFSs of H_2/air measured by different groups [80–95]. These data were measured at NTP using the OPF method during the last two decades. For comparison, the LFSs predicted by the chemical mechanism of Li et al. [73] are included. It is seen from Figure 2(a) that there is a very large discrepancy around 50 cm/s for the LFS of fuel-rich H_2/air mixtures. Moreover, Fig. 2(a) indicates that a low scatter appears at the fuel-lean side while a high scatter occurs at the fuel-rich side. This is because the definition of equivalence ratio is unevenly skewed for fuel-lean ($0 < \phi < 1$) and fuel-rich ($\phi > 1$) cases [22]. To address this, the normalized equivalence ratio, defined as $\phi/(1+\phi)$, was recommend by Law et al. [22]. Figure 2(b) shows that the scatter has similar magnitude for both fuel-lean and fuel-rich mixtures though the normalized equivalence ratio is used.

Figure 3 plots the LFSs of H_2/CO/air (H_2:CO=50%:50%) at NTP measured by different groups [90,92,96–104] using the OPF method, in which the predictions from the mechanism of Davis et al. [74] are included for comparison. Similar to H_2/air, Figure 3 shows that there are considerable discrepancies in LFSs measured for H_2/CO/air and that the asymmetry in the scatter can be reduced when the LFS is plotted against the normalized equivalence ratio proposed in [22].

Furthermore, Fig. 4 demonstrates the Markstein lengths relative to burned gas for H_2/air and H_2/CO/air mixtures at NTP. These data were also measured from the OPF method. Since the magnitude of Markstein length is relatively small, the observed discrepancy in Markstein length in Fig. 4 is much larger than that in LFS shown in Figs 2 and 3. This is consistent with the conclusion in the previous study [52], which shows that the Markstein length measured in the OPF method is very sensitive to extrapolation and has uncertainty about one-order larger than the LFS. Due to its large uncertainty, the Markstein length is not suggested as a target for validating and improving chemical mechanisms. In order to further examine the discrepancies in the LFSs measured by different groups [80–104], Figure 5 shows the normalized LFSs i.e. the ratio of reported LFSs, S_u^0, to the value predicted by simulation, $S_{u,\text{PREMIX}}^0$, at the same equivalence ratio. It is seen that for both H_2/air and H_2/CO/air mixtures with the equivalence ratio in the range of $1 < \phi < 3$, the relative difference is within 10%. However, for very rich mixtures, the relative difference can reach 20%. For fuel-lean H_2/air mixtures with $\phi < 0.8$, the deviation is enlarged and shown in Fig. 6. It is observed that the relative difference is above 50% for $\phi < 0.5$. These results indicate that the discrepancies in LFS measurement using the OPF method are considerable even for H_2/air and H_2/CO/air mixtures at NTP. Similar results were reported for CH_4/air mixtures at NTP in [29]. Therefore, we still need to make great efforts to improve the accuracy of the LFS of H_2/air, H_2/CO/air and CH_4/air mixtures measured using the OPF method.

As mentioned before, it is infeasible to employ LFS data with large uncertainties to restrain the uncertainty of chemical mechanisms for

Table 1
Experimental studies on laminar flame speed measurement of H_2/air [80–95] and H_2/CO/air [90,92,96–104] at NTP using the OPF method.

Fuel	No.	T_u(K)	P	ϕ	Extrapolation model	Data used in extrapolation[a]	Chamber[b]	Notes	Ref.
H_2	1	296	1 atm	0.3–5.0	Eq. (3)	$R_f \leq 3.5$ cm	Spherical, $R_w = 30$ cm	N2	Taylor, 1991 [80]
	2	298	1 atm	0.3–5.0	Eq. (3)	$R_f \leq 3.0$ cm	Spherical, $R_w = 18$ cm	N2	Aung, 1997 [81]
	3	298	1 atm	0.5–4.0	Eq. (3)	$R_f \leq 2.5$ cm	Cylindrical, $R_w = 4.13$ cm, $L = 12.7$ cm	N2	Tse, 2000 [82]
	4	298	1 atm	0.6–4.5	Eq. (3)	$R_f \leq 3.0$ cm	Spherical, $R_w = 18$ cm	N1	Kwon, 2001 [83]
	5	298	0.1 MPa	0.28–3.75	Eq. (3)	$R_f \leq 1.15$ cm	Spherical, $R_w = 12.5$ cm	N2	Lamoureux, 2003 [84]
	6	300	0.1 MPa	0.3–1.1	Eq. (3)	$R_f \leq 1.0$ cm	Spherical, $R_w = 19$ cm	N2	Verhelst, 2005 [85]
	7	300	0.1 MPa	0.6–1.4	Eq. (3)	$0.6 \leq R_f \leq 2.5$ cm	Cylindrical, $R_w = 4.13$ cm, $L = 12.7$ cm	N2	Huang, 2006 [86]
	8	365	0.1 MPa	0.3–1.0	Eq. (3)	N.A.	Spherical, $R_w = 9.5$ cm	N2	Bradley, 2007 [87]
	9	298	1 atm	0.6–1.6	Eq. (3)	$0.5 \leq R_f \leq 2.5$ cm	Cylindrical, $R_w = 9$ cm, $L = 21$ cm	N2	Tang, 2008 [88]
	10	298	1 atm	0.5–4.5	Eq. (3)	$0.5 \leq R_f \leq 2.5$ cm	Cylindrical, $R_w = 9$ cm, $L = 21$ cm	N2	Hu, 2009 [89]
	11	298	1 atm	0.6–5.5	Eq. (3)	$1.2 \leq R_f \leq 3$ cm	Cylindrical, $R_w = 10$ cm, $L = 15.24$ cm	N3	Burke, 2009 [90]
	12	293	0.1 MPa	0.3–5.6	Eq. (3)	N.A.	Spherical, $R_w = 25$ cm	N3	Kuznetsov, 2012 [91]
	13	298	1 atm	0.5–5.0	Eq. (3)	N.A.	Cylindrical, $R_w = 15.9$ cm, L =N.A.	N1	Krejci, 2013 [92]
	14	303	0.1 MPa	0.5–4.0	Eq. (3)	$0.8 \leq R_f \leq 2.5$ cm	Spherical, $R_w = 10$ cm	N3	Dayma, 2014 [93]
	15	298	1 atm	0.5–2.0	Eq. (4)	$0.7 \leq R_f \leq 2.1$ cm	Spherical, $R_w = 10$ cm	N2	Beeckmann, 2017 [94]
	16	296	0.1 MPa	0.8–3.5	Eq. (4)	$1.0 \leq R_f \leq 7.0$ cm	Spherical, $R_w = 28$ cm	N2	Grosseuvre, 2019 [95]
H_2/CO(1:1)	1	298	1 atm	0.6–4.4	Eq. (3)	$R_f \leq 3.5$ cm	Spherical, $R_w = 30$ cm	N2	McLean, 1994 [96]
	2	298	1 atm	0.6–5.0	Eq. (3)	$0.5 \leq R_f \leq 3.0$ cm	Spherical, $R_w = 18$ cm	N1	Hassan, 1997 [97]
	3	298	1 atm	0.6–4.0	Eq. (3)	$R_f \leq 2.5$ cm	Cylindrical, $R_w = 4.13$ cm, $L = 12.7$ cm	N2	Sun, 2007 [98]
	4	302 ± 3	0.1 Mpa	0.6–3.5	Eq. 3)	$0.5 \leq R_f \leq 6.2$ cm	Cylindrical, $R_w = 19.1$ cm, $L = 38.1$ cm	N2	Prathap, 2008 [99]
	5	298	1 atm	0.6–4.0	Eq. (3)	$1.2 \leq R_f \leq 3$ cm	Cylindrical, $R_w = 10$ cm, $L = 15.24$ cm	N3	Burke, 2009 [90]
	6	295 ± 4	0.1 MPa	0.4–5.0	Eq. (4)	$1.7 \leq R_f \leq 2.3$ cm	Cylindrical, $R_w = 8$ cm, $L = 30$ cm	N2	Bouvet, 2011 [100]
	7	298	1 atm	0.6–3.0	Eq. (4)	$0.8 \leq R_f \leq 3.0$ cm	Spherical, $R_w = 18$ cm	N1	Singh, 2012 [101]
	8	298	1 atm	0.5–4.0	Eq. (3)	N.A.	Cylindrical, $R_w = 15.9$ cm, L =N.A.	N2	Krejci, 2013 [92]
	9	298	0.1 MPa	0.6–4.0	Eq. (3)	$1.0 \leq R_f \leq 2.0$ cm	Cylindrical, $R_w = 5$ cm, $L = 30.5$ cm	N3	Ai, 2014 [102]
	10	298	0.1 MPa	0.4–1.0	Eq. (3)	$0.6 \leq R_f \leq 2.0$ cm	Cylindrical, $R_w = 5$ cm, $L = 14$ cm	N2	Li, 2014 [103]
	11	298	1 atm	0.5–0.9	Eq. (4)	$1.0 \leq R_f \leq 4.0$ cm	Spherical, $R_w = 12.5$ cm	N2	Gong, 2019 [104]

Notes: N1: The LFS data were from a table in this paper. N2: The LFS data were extracted from the corresponding figure in this paper. N3: The LFS data were provided by the authors of this paper. [a]The choice of flame radius range depends on the value of equivalence ratio. [b]R_w and L are the inner radius of spherical/cylindrical chamber and the length of cylindrical chamber, respectively.

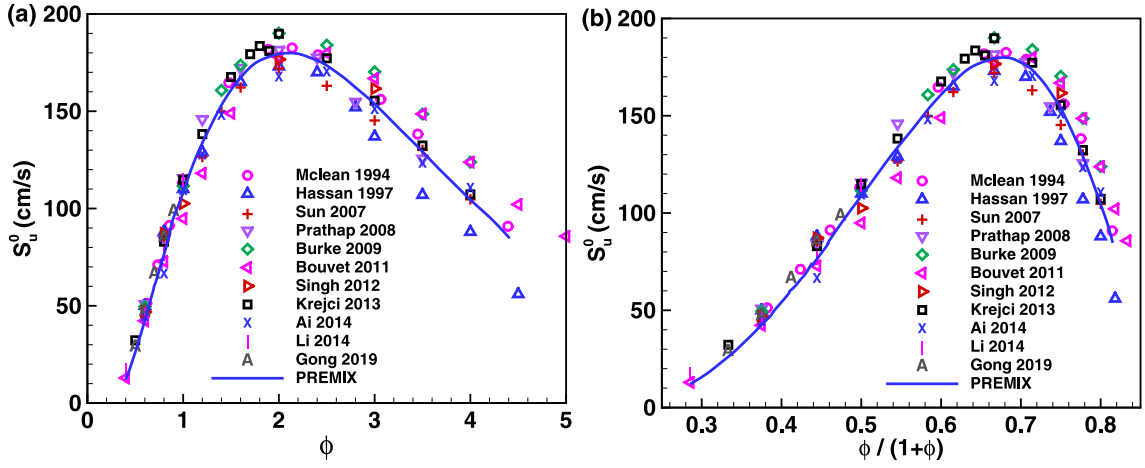

Fig. 3. Laminar flame speed of H_2/CO/air (H_2:CO=50%:50%) at NTP as a function of equivalence ratio (a) and normalized equivalence ratio (b). The symbols denote experimental results from [90,92,96–104]. The line denotes numerical results predicted by the mechanism of Davis et al. [74] using CHEMKIN-PREMIX code [105].

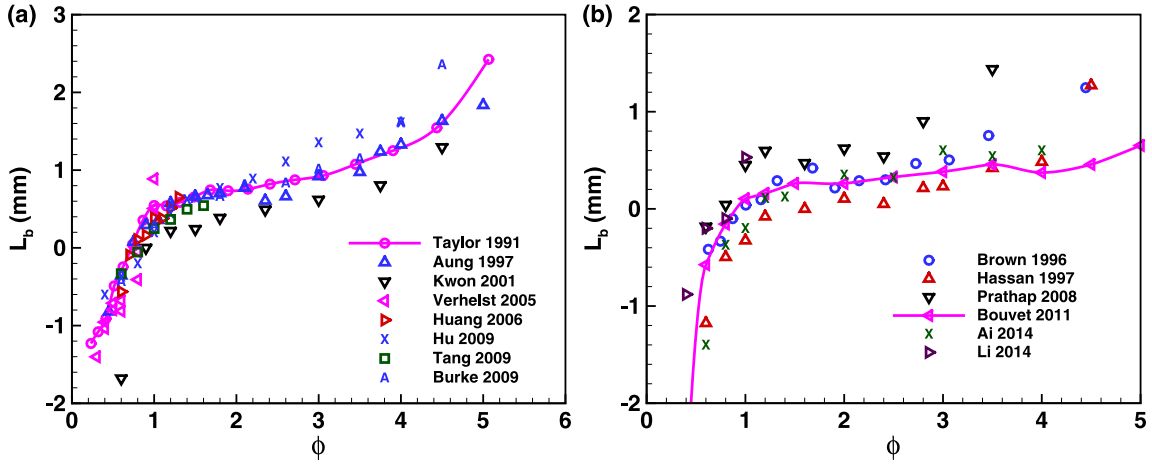

Fig. 4. Markstein length relative to burned gas for (a) H_2/air and (b) H_2/CO/air (H_2:CO=50%:50%) at NTP measured from the OPF method.

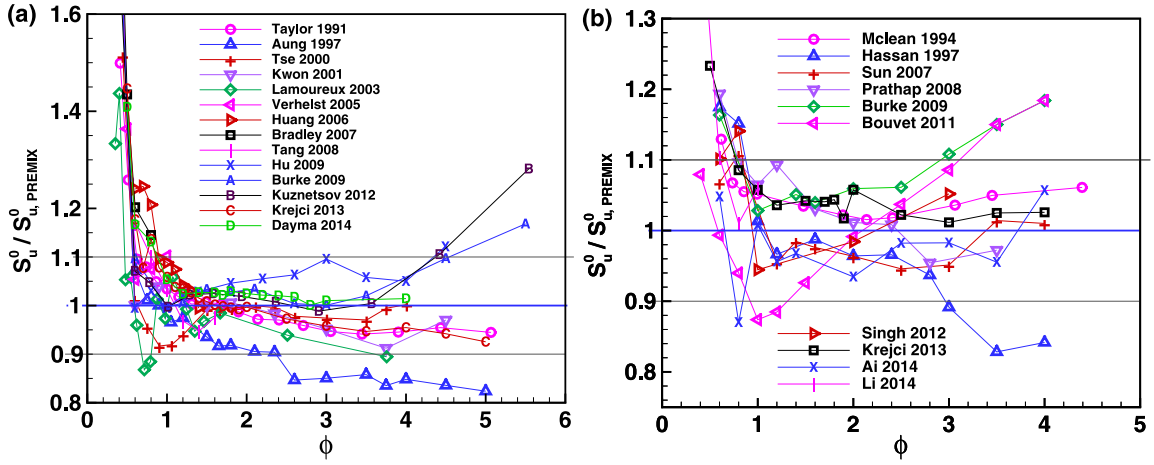

Fig. 5. Deviation of S_u^0 measured by different groups [80–93,96–103] from that predicted by simulation, $S_{u,\mathrm{PREMIX}}^0$ based on the mechanism of Li et al. [73] for (a) H_2/air and the mechanism of Davis et al. [74] for (b) H_2/CO/air (H_2:CO=50%:50%) at NTP.

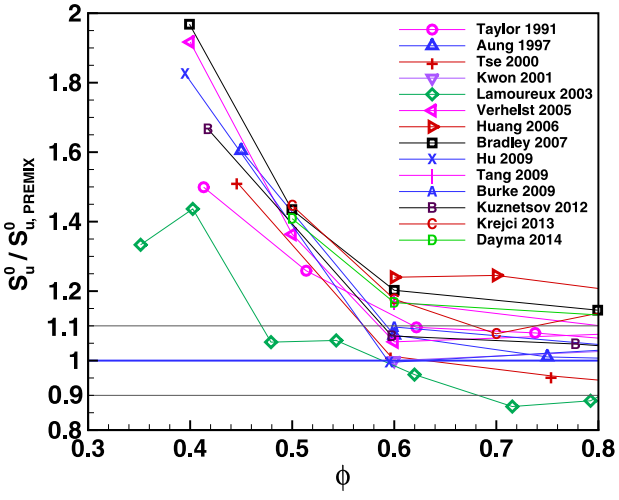

Fig. 6. Deviation of S_u^0 measured by different groups from that predicted by simulation, $S_{u,\mathrm{PREMIX}}^0$ based on the mechanism of Li et al. [73] for lean H_2/air at NTP.

hydrogen and syngas. This is because the sensitivity of LFS to key elementary reaction rates is relatively lower than ignition delay time. Figure 7(a) shows the sensitivity of LFS to the kth elementary reaction rate, S_K, for H_2/air. The sensitivity is defined as $S_K = \frac{\partial \ln(S_u^0)}{\partial \ln(A_K)}$, where A_K is the A-factor in the formulation of S_K [105]. Relatively low sensitivity of LFS to key elementary reactions is observed in Fig. 7(a). Moreover, the most sensitive elementary reactions, R1 ($H+O_2 \rightleftharpoons O+OH$) and R4 ($H+O_2+M \rightleftharpoons HO_2+M$), both have low uncertainties. Besides the sensitivity, the uncertainty in elementary reaction rate needs to be considered. Furthermore, a sensitivity-weighted uncertainty momentum [106] is employed to include both sensitivity and uncertainty, which is defined as $\sigma_K = S_K \times (f_K - 1)$ where f_K is the uncertainty factor of the kth elementary reaction. Figure 7(b) shows that σ_K of key elementary reactions is within 20%. Moreover, the magnitudes of σ_K are within 10% for the most important elementary reactions, i.e., R1 ($H+O_2 \rightleftharpoons O+OH$) and R4 ($H+O_2+M \rightleftharpoons HO_2+M$). Note that similar results are also observed for H_2/CO/air. Therefore, it is not accessible to reduce the uncertainty in the elementary reaction rates by using the existing LFS data with large discrepancies. This suggests that high-quality experimental LFS data are still required to achieve reliable validation and improvement of chemical mechanisms.

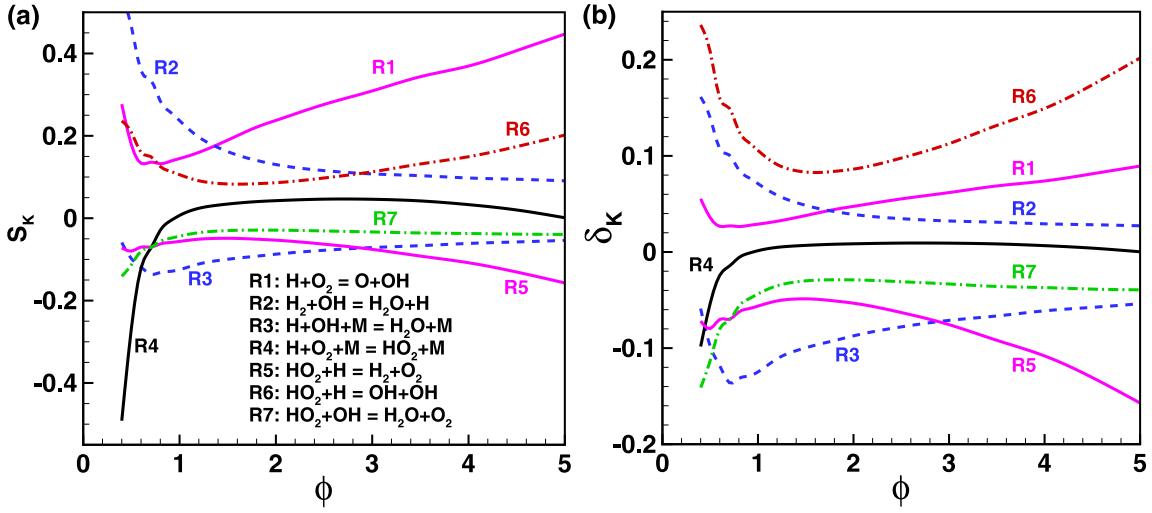

Fig. 7. (a) Sensitivity coefficient, S_K, and (b) sensitivity-weighted uncertainty momentum, σ_K, as a function of equivalence ratio for laminar flame speed of H_2/air at NTP. $\sigma_K = S_K \times (f_K - 1)$[106] and f_K is the uncertainty factor of kth elementary reaction ($f_K = 1.2$ for R1 and R4; $f_K = 1.3$ for R2; $f_K = 2.0$ for R3, R5, R6, and R7) [74].

4. Sources of uncertainty in LFSs

In this section, we aim to identify the possible sources of uncertainty in the LFSs measured using the OPF method for hydrogen/air and syngas/air at NTP. As suggested by previous studies [16,29], the underlying sources could include (a) how mixtures are prepared, (b) ignition effects, (c) flame instability and radiation, chamber confinement, and buoyancy, and (d) nonlinear stretch behavior and the performance of extrapolation models. It is noted that these sources are inherently coupled each other, especially at large flame radii. It remains a formidable challenge to obtain experiments data at large flame radius due to the flame instability during its propagation in air and limitation of imaging capability. Therefore, OPF simulations are conducted since the numerical method can help to isolate and examine different sources of uncertainty individually. Unless otherwise specified, the data presented in Figs 8–19 in this section are provided by the OPF simulations.

4.1. Mixture preparation

To obtain high-quality LFS data from the OPF method, we need to diminish the influence of different factors which could affect the accuracy of LFS measurement. As indicated in Table 1, the LFSs were not measured at exactly the same initial conditions of $T_u = 298$ K and $P = 1$ atm. For example, the initial temperature can be in the range of 298 ± 3 K or 298 ± 5 K, and the initial pressure can be $P = 0.1$ MPa. Besides, a partial pressure method is usually used to prepare combustible mixture. The uncertainty in the mixture composition or equivalence ratio always exists and it is non-negligible especially when a pressure gauge with low accuracy is used in experiments [21,29,106,107].

Figure 8 shows the effects of mixture preparation on the propagation speed of a spherical H_2/air flame. The results are obtained from simulations using A-SURF and the mechanism of Li et al. [73]. The data in Fig. 8(a) show that the change in flame speed is around 1% when the equivalence ratio is changed by 0.01. Since Fig. 2(a) shows that the gradient, $dS_u^0/d\phi$, reaches its maximum value for ϕ around 1.0, the uncertainty in LFS due to mixture composition is expected to be lower at fuel-leaner or fuel-richer conditions. Furthermore, compared to hydrocarbon/air at the same equivalence ratio, the fuel/air molar ratio for hydrogen and syngas is much higher. This results in a lower uncertainty in fuel concentration for hydrogen and syngas. Therefore, the uncertainty in the mixture composition or equivalence ratio has little contribution to the uncertainty in LFSs measured for hydrogen and syngas.

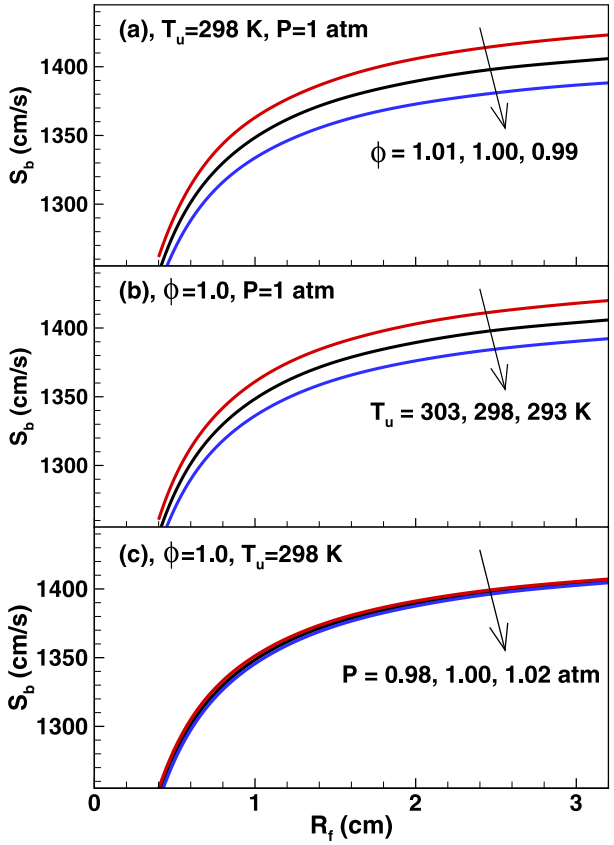

Fig. 8. Effects of mixture preparation on the spherical flame propagation in H_2/air.

Figure 8 (b) shows that the change in flame speed is around 1% when the initial temperature is perturbed by ±5 K. On the other hand, it is found from Fig. 8(c) that for the perturbation in the initial pressure, nearly identical flame propagation speeds (the relative difference is within 0.1%) are obtained. Compared to the large discrepancies shown in Fig. 5, the uncertainty in LFS caused by the mixture preparation (slight perturbation in equivalence ratio, initial temperature or pres-

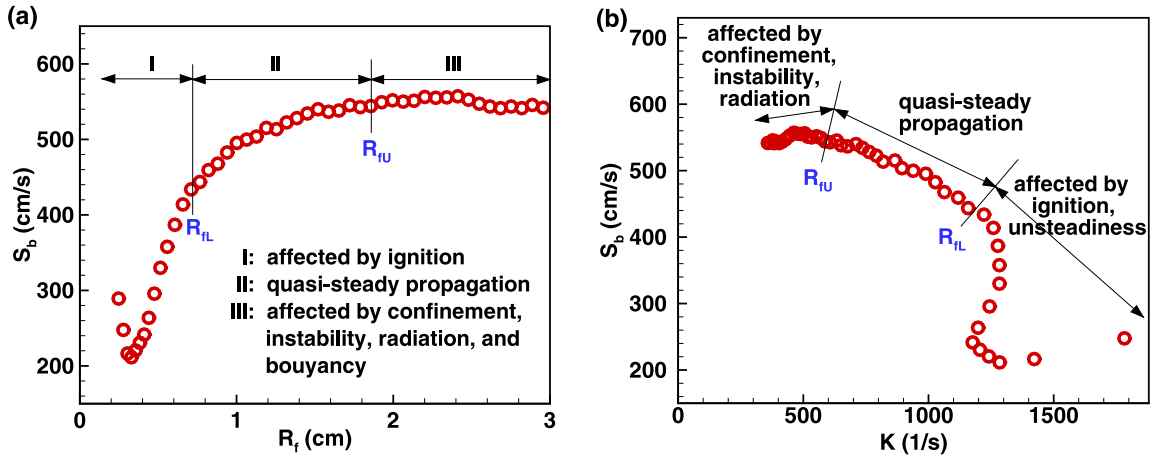

Fig. 9. Change of stretched flame speed S_b with (a) flame radius R_f and (b) stretch rate K for fuel-rich H2/air ($\phi = 4.5$) at NTP. These experimental data are from [53].

sure) is almost negligible. It is noted that recently Zhang et al. [108] has shown that the accuracy of LFS measurement can also be affected by the non-uniform initial temperature distribution inside the closed chamber. At NTP, there is no preheating and thereby the initial temperature is uniform. However, for LFS measurements at elevated temperatures, the non-uniformity in initial temperature should be diminished.

Figure 9 plots the stretched flame speed obtained from numerical differentiation of the flame front history via $S_b = dR_f/dt$. For the spherical flame with small radius in regime I, $R_f < R_{fL}$, the stretched flame speed changes non-monotonically with the flame radius and stretch rate. In this regime, the spherical flame propagation is strongly affected by ignition [53,86,109–113]. On the other hand, the spherical flame with large radius in regime III, $R_f > R_{fU}$, could be affected by confinement [90,114–116], flame instability [87,117–120], radiation [56,115,121–128] and/or buoyancy [129–133]. The LFS can only be obtained based on experimental data in regime II, in which quasi-steady propagation of spherical flame occurs. Therefore, $R_{fL} < R_f < R_{fU}$ is the appropriate flame radius range that should be used in the data processing to obtain the LFS. However, it is difficult to choose the proper values for the lower and upper bounds, $R_{fL}$and R_{fU}, which are affected by ignition, confinement, flame instability, radiation and buoyancy. Furthermore, even after R_{fL} and R_{fU}, are properly determined, the accuracy of LFS is still affected by nonlinear stretch behavior [50–52,134–138] and extrapolation based on data in regime II [139–141]. In the following, different factors in regimes I, III, and II are discussed.

4.2. Ignition effects in regime I

A large ignition energy is needed to successfully initiate a spherical flame in a fuel-rich H_2/air mixture due to its relative large effective Lewis number [142–145]. Consequently, rich H_2/air mixtures have relatively large critical flame radii above which the ignition effects can be negligible. Figure 10 shows the change of stretched flame speed with flame radius and stretch rate for a fuel-rich H_2/air mixture with $\phi = 4.5$. The spherical flame is initiated by three ignition energies. Both the experimental and numerical results show that the ignition energy has a great impact on the initial spherical flame propagation. The different flame speed trajectories converge onto a single curve only when the flame radius is above a critical value donated by R_C [53]. Therefore, the lower radius bound, R_{fL},should be greater than the critical radius R_C. Otherwise the accuracy of LFS measurement would be affected by ignition. Figure 11 shows the change of critical flame radius with the equivalence ratio for H_2/air at NTP. The critical flame radius depends strongly on the equivalence ratio. For fuel-rich H_2/air, the critical radii are 7 mm and 12 mm for $\phi = 4.5$ and $\phi = 5.5$, respectively. Therefore, for fuel-rich H_2/air the lower radius bound, R_{fL}, should be larger than 10 mm, which is well above the value of $R_{fL} = 6$ mm suggested by Bradley and co-workers [109,146]. The critical flame radius for syngas/air is expected to be lower than that for hydrogen/air. Nevertheless, the lower radius bound (R_{fL}) should be properly chosen to avoid the ignition effect, especially for hydrogen-rich syngas.

4.3. Confinement, instability, radiation and buoyancy effects in regime III

For the LFSs measured for H_2/air and H_2/CO/air, all the groups [80–104]listed in Table 1 assumed that the burned gas is static, i.e., $u_b = 0$, and thereby $S_b = dR_f/dt$. However, as indicated in Fig. 9, confinement could affect spherical flame propagation in regime III with $R_f > R_{fU}$ [90,114–116]. This is due to the fact that an inward flow is caused by the confinement effect when the flame radius is large than R_{fU} [94]. This inward flow is able to slow down the spherical flame propagation. This is demonstrated by Fig. 12, which shows that the stretched flame speed without flow correction changes non-monotonically with the stretch rate. A lower LFS will be obtained from extrapolation based on the data affected by confinement. To obtain accurate LFSs from spherical flames with large radii, flow correction should be conducted [90]. Figure 12 shows that after flow correction, the stretched flame speed changes almost linearly with the stretch rate. It was recommended that in order to reduce the influence of confinement, the upper radius bound, R_{fU}, should be within 30% of the (equivalent) chamber radius [29,90,114]. In most of the studies listed in Table 1, the upper radius bound, R_{fU}, chosen in data processing is less than 30% of the (equivalent) chamber radius. Therefore, the effects of confinement on the LFSs measured for H_2/air and H_2/CO/air listed in Table 1 are negligible. It is noted that confinements effects play a major role for cylindrical chambers as described in [90].

Radiation from high-temperature burned gas always exists during spherical flame propagation. The larger the spherical flame radius are, the longer the radiating time of burned gas has. Therefore, as indicated in Fig. 9, radiation has the ability to affect spherical flame propagation in regime III with $R_f > R_{fU}$ [56,115,121–128]. Radiation can not only reduce the flame temperature but also induce inward flow of burned gas, both of which slow down the spherical flame propagation [128]. The radiation induced flame speed reduction strongly depends on the flame speed itself since the radiating time is inversely proportional to the flame propagation speed. The larger the flame propagation speed is, the shorter the radiating time is and thus the weaker the radiation effect is. Therefore, radiation effect is expected to be small for H_2/air and H_2/CO/air mixtures which have larger LFSs than hydrocarbon fuels. The radiation relative reduction in LFS for H_2/air and H_2/CO/air

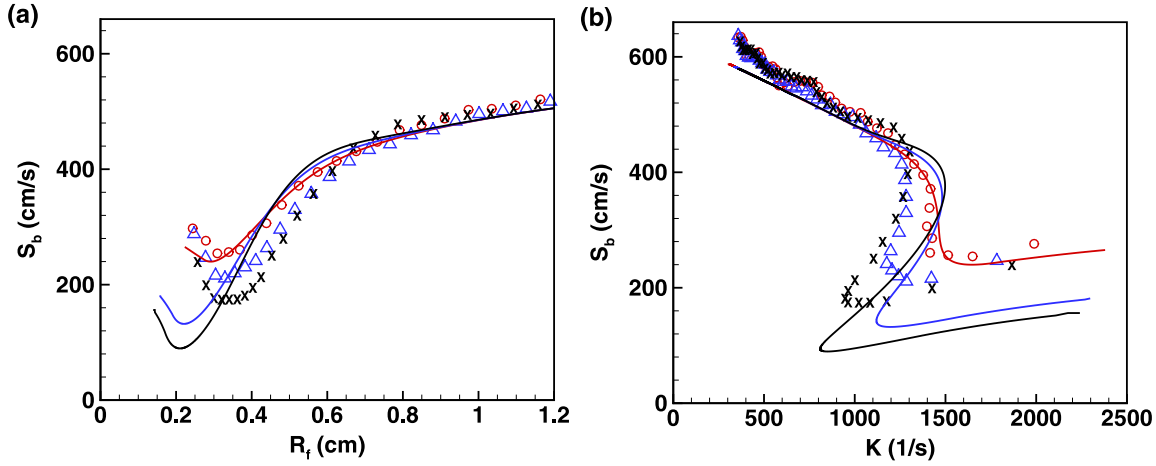

Fig. 10. Change of stretched flame speed S_b with (a) flame radius R_f and (b) stretch rate K for fuel-rich H_2/air ($\phi = 4.5$) at NTP. The symbols denote experimental data in [53] and the lines represent simulation results. Three ignition energies were used in both experiments and simulations.

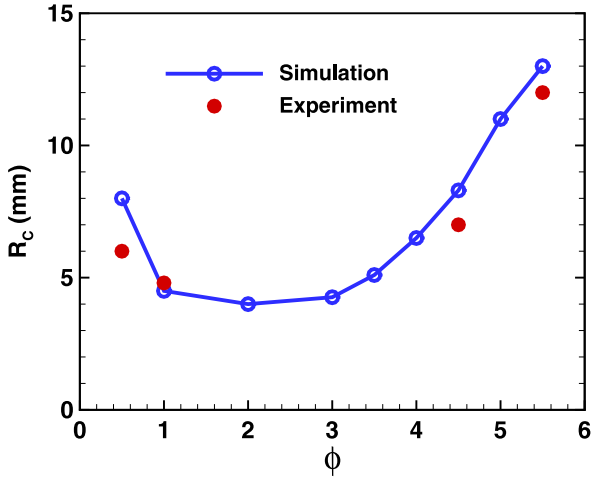

Fig. 11. Change of critical flame radius (R_c) with the equivalence ratio (ϕ) for H_2/air at NTP. Adapted from [53].

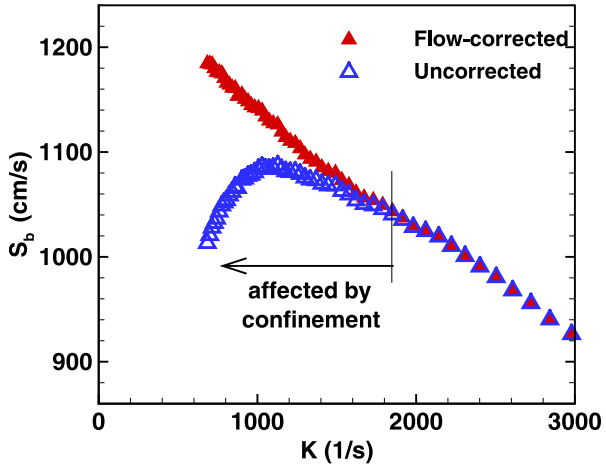

Fig. 12. The stretched flame speeds (S_b) with and without flow correction for fuel-rich H_2/air ($\phi = 3$) as a function of stretch rate (K) at NTP. Adapted from [90].

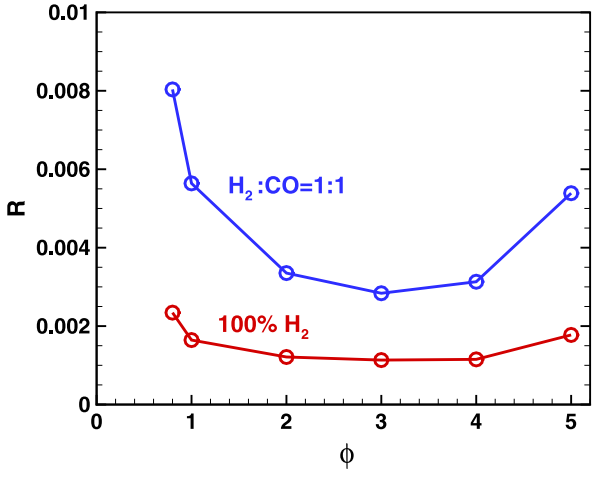

Fig. 13. Radiation induced relative reduction (R) in LFS for H_2/air and H_2/CO/air (H_2:CO=50%:50%) as a function of equivalence ratio (ϕ) at NTP. Adapted from [123].

(H_2:CO=50%:50%) at NTP is shown in Fig. 13. It is seen that the influence of radiation is within 1% and 0.3% for H_2/CO/air and H_2/air, respectively. Therefore, the discrepancies in LFSs shown in Section 2 is not caused by radiation effect.

Ronney and Wachman [147] showed that the spherical flame propagation speeds are almost identical at one-g and zero-g when $S_u^0 >$ 15 cm/s. Since the LFSs of H_2/CO/air and H_2/air are much higher than 15 cm/s, the contribution of buoyancy to the discrepancies in LFSs shown in Section 2 is negligible. Besides, the upper radius bound, R_{fU}, is usually chosen so that the cellular instability does not develop over the flame surface. This ensures that the accuracy of LFS measurement is not affected by flame instability when the OPF method is used [87].

4.4. Extrapolation based on data in regime II

In the previous two sub-sections, different factors including ignition, confinement, flame instability, radiation and buoyancy are discussed since they could affect the lower and upper bounds, R_{fL} and R_{fU}, of regime II. In this sub-section, the extrapolation of LFS based on data in regime II is discussed.

As mentioned in Section 2, the unstretched flame speed relative to the burned gas, S_b^0, can be obtained from linear or nonlinear models

Table 2
Different models used in extrapolation.

Model	Expression	Notes	Ref.
LS	$S_b = S_b^0 - L_b K$	**L**inear model based on **S**tretch	[45]
LC	$S_b = S_b^0(1 - L_b\kappa)$	**L**inear model based on **C**urvature	[148]
NQ	$\left(\frac{S_b}{S_b^0}\right)^2 \ln\left(\frac{S_b}{S_b^0}\right)^2 = -\frac{2L_b K}{S_b^0}$	**N**onlinear **Q**uasi-steady model	[50]
N3P	$\frac{S_b}{S_b^0} = 1 - L_b\kappa + \frac{C}{R_f^2}$	**N**onlinear model with **3** **P**arameters	[135]
NE	$\frac{S_b}{S_b^0}\left[1 + L_b\kappa + (L_b\kappa)^2 + \frac{2}{3}(L_b\kappa)^3\right] = 1$	**N**onlinear model in **E**xpansion form	[134]
FTE	$\left(\frac{S_b}{S_b^0} + \delta^0\kappa\right)\ln\left(\frac{S_b}{S_b^0} + \delta^0\kappa\right) = -(L_b - \delta^0)\kappa$	**F**inite flame **T**hickness **E**xpression	[137]
NL4	$\frac{S_b}{S_b^0} = 1 - \frac{\delta^0\kappa S_b^0 L_b}{S_b} + \left(\frac{\delta^0\kappa S_b^0 L_b}{S_b}\right)^2 - \left(\frac{\delta^0\kappa S_b^0 L_b}{S_b}\right)^3$	**N**on-**L**inear model	[149]
NQH	$\left(\frac{S_b}{S_b^0}\right)^2 \ln\left(\frac{S_b}{S_b^0}\right)^2 = -\frac{2L_b K}{S_b^0} + \frac{C}{R_f^2}$	**NQ** model with a **H**igh-order term	**This work**

given by Eqs. (3) and (4), respectively. The LFS is then determined through $S_u^0 = \sigma S_b^0$, where σ is the density ratio. Besides these two models, several models have been developed recently, including a new model- NQH – proposed in this work. These models are summarized in Table 2. The first three models, LS, LC and NQ are accurate to the first-order in terms of the inverse of flame radius [52]. Models N3P and NQH are accurate to the second-order in terms of the inverse of flame radius, while models NE and NL4 have the accuracy to the third-order. Unlike other models, the models NL4 and FTE include the flame thickness δ^0as a fitting parameter. Model LS is popularly used by different groups. Models LC and NQ were proposed for mixtures with $Le > 1$ while other models were for mixtures with $Le < 1$, for both of which strong nonlinear stretch behavior may occur. For hydrogen and hydrogen-rich syngas, the effective Lewis number becomes apparently larger/smaller than unity at fuel-rich/fuel-lean conditions. In the following we first consider fuel-rich case with $Le > 1$. In this context, the advantage and deficiency of the NQH model are summarized as follows. Compared to the first-order LS, LC and NQ models, NQH is accurate to the second-order and can be implemented more easily than the NL4 and FTE models. Moreover, it is found that as pressure increases the NQH model could be more accurate than the second-order N3P model (see Fig. 18). While the NQH model has significant advantages over other models, it is a relatively lower order model than the third-order NE and NL4 models.

Figure 14 shows the results for a fuel-rich H2/air mixture ($\phi = 4.5$), whose effective Lewis number is around 2.1 [15]. The laminar flame speeds, S_b^0, and Markstein lengths, L_b, from linear extrapolations based on three models, LS, LC, and NQ, and two flame radius ranges, $1 < R_f < 2$ cm and $0.5 < R_f < 2$ cm, are presented. It is observed that when the same flame radius range is used, S_b^0 and L_b extracted by different models decrease in the order of LS, LC, and NQ. When the flame radius range of $0.5 < R_f < 2$ cm is used in extrapolation (dashed lines in Fig. 14, the maximum relative difference for S_b^0 and L_b is $727.7/616.9 - 1 = 18\%$ and $2.59/0.88 - 1 = 194\%$, respectively. Thus, the extracted results, especially the Markstein length, strongly depend on the model used in extrapolation. Regarding the effects of flame radius range on the extracted S_b^0 and L_b, Fig. 14 indicates that the nonlinear extrapolation based on LC or NQ is much less sensitive to the flame radius range than that based on LS. Therefore, use of LC or NQ instead of LS in linear extrapolation can reduce the influence of flame radius and thereby reduce the uncertainty in LFS measurement for fuel-rich H_2/air mixtures.

The above observation is further demonstrated by Fig. 15(a), in which the extracted results from different models using different flame radius ranges, $R_{fL} < R_f < R_{fU}$, are plotted for H_2/air at $\phi = 4.5$. Figure 15(a) shows that the extracted laminar flame speed and Markstein length strongly depend on the flame radius range and the extrapolation model. Moreover, the results show that use of LC or NQ yields extracted flame properties that are more consistent and less sensitive to flame radius range than use of LS. Unlike the fuel-rich hydrogen/air mixture, the results for the stoichiometric case ($\phi = 1.0$) shown in Fig. 15(b) indicate that neither the extrapolation model nor the flame radius range has obvious influence on the extracted results. This is because the effective Lewis number for stoichiometric H_2/air is close to unity.

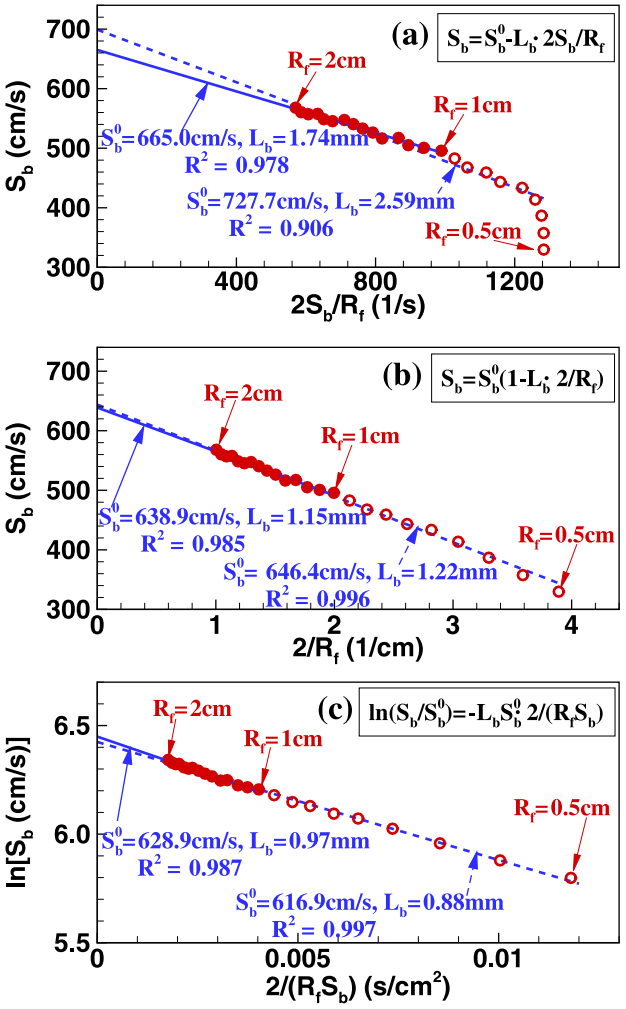

Fig. 14. Extrapolation of the laminar flame speed S_b^0 and Markstein length L_b for H_2/air mixture ($\phi = 4.5, T_u = 298$ K, $P = 1$ atm). The symbols denote experimental data. The solid and dashed lines denote linear extrapolations using flame radius range of [1 cm, 2 cm] (only closed symbols) and [0.5 cm, 2 cm] (all symbols), respectively.

The above results indicate that for fuel-rich H_2/air and H_2/CO/air mixtures with $Le > 1$, large uncertainty can be caused by extrapolation, especially when the LS model is used. As shown in the following, this becomes even worse for fuel-lean case with $Le < 1$. Figure 16 shows simulation results for a fuel-lean H_2/air mixture ($\phi = 0.4$), whose effective Lewis number is around 0.5 [15]. It is noted that in fuel-lean H_2/air experiments, cellular instability appears and usually data with $R_f > 1.5$ cm cannot be used to obtain the LFS [87]. However, in simulation the OPF

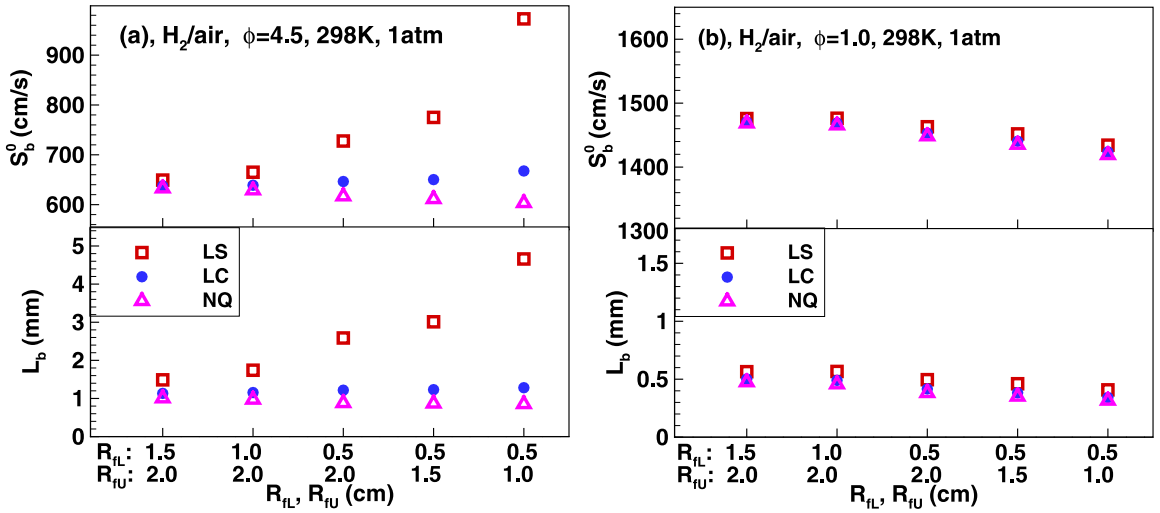

Fig. 15. Laminar flame speeds and Markstein lengths extrapolated using different models and flame radius ranges $[R_{fL},R_{fU}]$ for H_2/air mixtures.

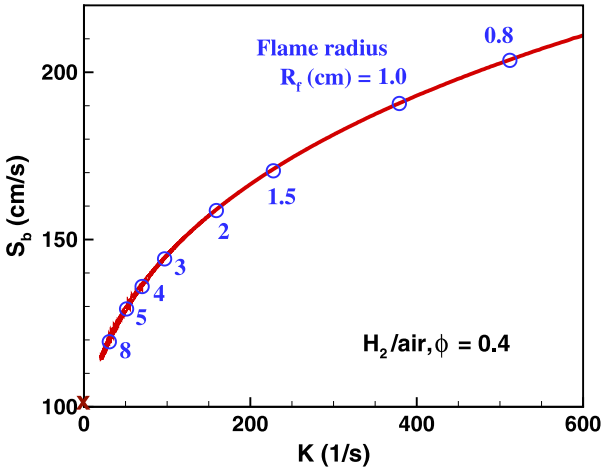

Fig. 16. Stretched flame speed S_b as a function of stretch rate K for fuel-lean H_2/air ($\phi = 0.4$) at NTP. The cross symbol denotes the unstretched LFS.

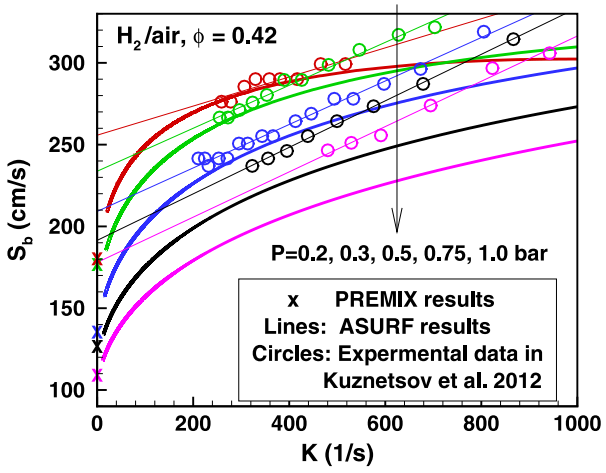

Fig. 17. Stretched flame speed as a function of stretch rate for fuel-lean H_2/air ($\phi = 0.42$) at different pressures of $P = 0.2$, 0.3, 0.5, 0.75 and 1.0 bar. The symbols denote experimental results measured from OPF by Kuznetsov et al. [91]. The thin straight lines detonate linear fitting of the experimental data. The thick curves denote numerical results from ASURF. The cross symbols denote the unstretched LFSs.

is one-dimensional and there is no cellular instability. Very strong nonlinear behavior between S_b and K is observed in Fig. 16. Extrapolation based on data in the range of $0.8 \le R_f \le 1.5$ cm yields $S_b^0 \approx 150$ cm/s. However, a much smaller value of $S_b^0 \approx 100$ cm/s can be obtained for extrapolation based on flames with $5 \le R_f \le 8$ cm. Consequently, the LFSs measured from OPF experiments for lean hydrogen and syngas are much larger than the correct values since the small flame radius range of $0.8 \le R_f \le 1.5$ cm should be used to avoid cellular instability [135,136]. Even the nonlinear extrapolation is used, large discrepancies between experiments and model predictions still exists for lean H_2/air [135,136]. This explains the large discrepancies for lean both H_2/air and H_2/CO/air shown in Figs. 5 and 6.

Recently, Liang et al. [137] has proposed to consider the flame thickness in the extrapolation based on the nonlinear model in [142,144]. However, the discrepancy cannot be diminished, especially for low pressures. Kuznetsov et al. [91] and Dayma et al. [93] measured the LFS of lean H_2/air at $P = 0.2$ bar. Comparison between the experimental data from [91]and simulation results is shown in Fig. 17. It is seen that nonlinear behavior between S_b and K becomes stronger at lower pressures. Consequently, the LFS is greatly over-predicted by extrapolation based on limited experimental points and it strongly depends on the linear/nonlinear model and flame radius range used in extrapolation.

To further investigate the nonlinear behavior effect at lower pressures, the simulation results obtained by A-SURF are used to examine the performance of different extrapolation models for determining the unstretched flame speed S_b^0, which is shown in Fig. 18. In the simulations, a large chamber radius is considered for avoiding the confinement effect, and data used for fitting is for flame radius from 1 cm to 2 cm. It is noted that previous investigation by Wu et al. [135] demonstrated that the N3P model is better than the NE/NQ models for H_2/air considered here. Therefore, the performance of the NQH model is directly compared with the N3P in Fig. 18. It is seen that for room pressure (i.e. 1 bar) both the N3P and NQH models have the potential to reproduce the simulation results, performing better than the LS and LC models, as expected. However, for lower pressures (i.e., 0.2 bar and 0.5 bar), significant difference between model predictions and simulation results is observed, which means none of the models are valid for lower pressure cases considered here. Furthermore, it is found that as pressure increases the NQH model proposed in this work could be more accurate than the other three models. The LFSs predicted by NQH/N3P are 35%/36%, 23%/29%, and

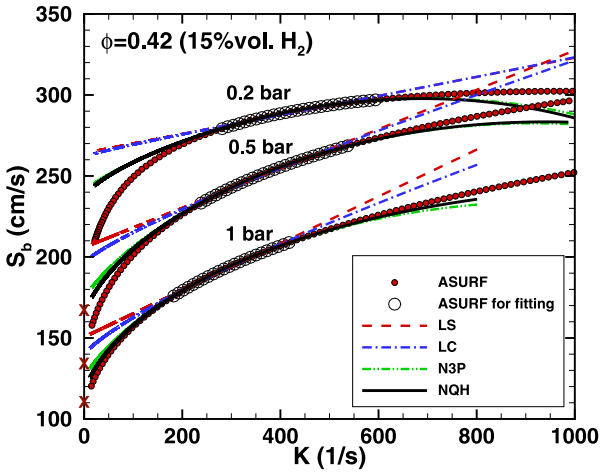

Fig. 18. Stretched flame speed as a function of stretch rate for fuel-lean H_2/air ($\phi = 0.42$) at different pressures of $P = 0.2$, 0.5 and 1.0 bar. The cross symbols denote the unstretched LFSs

9%/18% larger than PREMIX results at $P = 0.2$ bar, 0.5 bar, and 1 bar, respectively. The results from Figs. 17 and 18 suggest that further extrapolation model development is required for achieving accurate predicting laminar flame speeds at reduced pressure conditions.

Hydrogen/air and syngas/air mixtures have effective Lewis numbers apparently below and above unity respectively for fuel-lean and fuel-rich cases. The above analysis indicates that the uncertainty in LFS measured for H_2/air and H_2/CO/air from the OPF method is mainly due to nonlinear stretch behavior and extrapolation. In order to reduce the uncertainty associated with extrapolation, we should directly compare the measured stretched flame speeds with 1-D simulation results predicted by kinetics [29,56,136,139]. Figure 19 shows such comparison for stoichiometric H_2/air at NTP. It is observed in that the discrepancy in S_b at certain value of stretch rate can be larger than the discrepancy in S_b^0 at zero stretch rate obtained from linear extrapolation. Therefore, extrapolation might hide the discrepancy in raw experimental data. As suggested in [29,56,136,139], not only the extracted results (S_b^0 or S_u^0) but also the original data used for extrapolation (S_b versus Kor R_f) should be provided in future investigation.

5. Concluding remarks

In this work, the uncertainty of laminar flame speeds (LFSs) measured for hydrogen/air and syngas/air mixtures using outwardly propagating spherical flame (OPF) methods are reviewed. The experimental data reported in the literature are collected and compared simulation results considering with detailed chemistry and transport models. The sources of uncertainty in the LFSs are discussed in three flame regimes, I, II and III, in terms of flame radius and the main factors are identified through analysis of the experimental and numerical data. A new LFS extrapolation model – NQH – is proposed and compared with existing models. The following conclusions can be drawn based on this study:

- Due to the unevenly skewed definition of equivalence ratio, there is a low scatter at the fuel-lean side while a high scatter at the fuel-rich side. For fuel-lean case with equivalence ratio below 0.5, the relative discrepancy can reach 50%. The results shows that the Markstein length measured using the OPF method is very sensitive to extrapolation and has uncertainty about one-order larger than the LFS. Furthermore, the sensitivity-weighted uncertainty momentum is evaluated and it is found that the LFS data with large discrepancies cannot help to reduce the uncertainty in the rates of elementary reactions for hydrogen and syngas.
- The results suggest that the mixture preparation (i.e., slight perturbation in equivalence ratio, initial temperature or pressure) has a negligible impact on the uncertainty of the LFS. It is critical to choose an appropriate flame radius range ($R_{fL} < R_f < R_{fU}$) that would be used in the data processing to obtain the LFS. Based on the lower and upper bounds, R_{fL} and R_{fU}, the underlying sources of uncertainty are investigated in three regimes, regime I: $R_f < R_{fL}$; regime II: $R_{fL} < R_f < R_{fU}$; and regime III: $R_f > R_{fU}$.
- The contribution of ignition effects occurred in regime I to the uncertainty depends strongly on the equivalence ratio of hydrogen/air and syngas/air mixtures. Simulation results indicate that for fuel-rich H_2/air, the lower radius bound (R_{fL}) should be larger than 10 mm, which is well above the value of R_{fL} used in the literature listed in Table 1 and $R_{fL} = 6$ mm suggested by Bradley and coworkers [109,146]. In this context, the ignition effects in regime I could be one of the main sources of uncertainty in the LFSs measured for hydrogen/air and syngas/air mixtures using the OPF method.
- The impact of confinement, instability, radiation and buoyancy in regime III on the uncertainty in the LFSs is found to be negligibly small for hydrogen/air and syngas/air mixtures. This is due to the

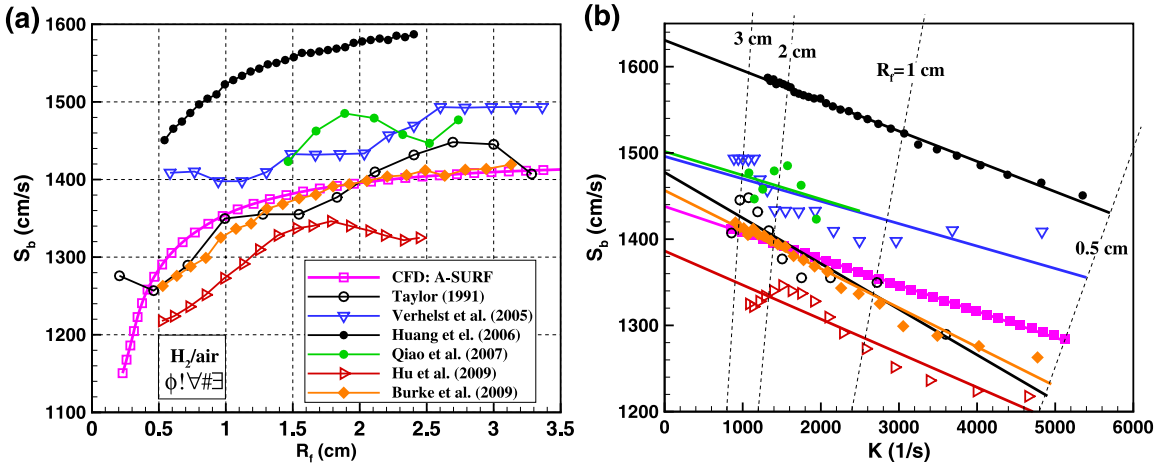

Fig. 19. Stretched flame speed as a function of flame radius (a) and stretch rate (b) for stoichiometric H_2/air at NTP. The symbols denote simulation results (pink square) or experimental data in the literature from OPF [80,85,86,89,90,150]. The solid lines stand for linear fitting and the dashed lines denote the flame radii contours (they are straight lines since $R_f = 2S_b/K$).

proper choice of the upper radius bound R_{fU} in the LFS measurements and a relatively larger the flame propagation speed.
- It is found that the accuracy of extracted LFS and Markstein length based on data in regime II is strongly affected by the choice of extrapolation model and the flame radius range for extrapolation. The nonlinear extrapolation based on LC or NQ models is much less sensitive to the flame radius range than that based on linear model – LS. Therefore, use of LC or NQ instead of LS in extrapolation can reduce the influence of flame radius and thereby reduce the uncertainty in LFS measurement, especially for fuel-rich ($Le > 1$) and/or fuel-lean ($Le < 1$) H_2/air and syngas/air mixtures. Nevertheless, strong nonlinear behavior between stretched flame speed and stretch rate still makes a major contribution to the very large discrepancies observed for fuel-lean/fuel-rich mixtures even when the nonlinear extrapolation models are used.
- A nonlinear extrapolation model NQH (including a high-order term in the NQ model) is considered to address the nonlinear stretch behavior. It is found that as pressure increases the NQH model could be more accurate than other models.

The current work focuses on the accuracy of LFSs measured from the OPF method for hydrogen/air and syngas/air at the normal temperature and pressure. The results indicate that great effort still needs to be devoted to reducing the uncertainty in the LFSs. Some recommendations are summarized below.

- When selecting the flame radius range for extrapolation, the lower radius bound (R_{fL}) should be properly chosen to avoid the ignition effect, especially for fuel-rich hydrogen/air and syngas/air mixtures which have relatively large critical flame radii above which the ignition effects are negligible. To determine the value of R_{fL}, multiple experiments can be conducted for the same mixture conditions at different ignition energies. The critical flame radius where the corresponding multiple flame speed trajectories converge onto a single curve could be used as R_{fL}.
- For very fuel-lean or fuel-rich hydrogen/air and syngas/air mixtures, the nonlinear extrapolation models (e.g., LC, NQ, and NQH) are recommended since they are much less sensitive to the flame radius range than the linear model LS. Furthermore, in order to reduce the uncertainty of chemical mechanism caused by extrapolation models, we should directly compare the measured stretched flame speeds with simulation results predicted by kinetics.
- Given the major contribution of extrapolation models to the uncertainty in the LFSs, the development of more advanced extrapolation models is indispensable for achieving accurate predictions of the LFSs of fuel-lean or fuel-rich hydrogen/air and syngas/air mixtures.
- Experimental databases at sub-atmospheric and elevated pressure conditions are needed to improve the predictability of the hydrogen or syngas chemical mechanisms over extensive ranges of pressure, which would bring a challenge with respect to extrapolation model development because the nonlinear nonlinear behavior between stretched flame speed and stretch rate is further augmented under reduced pressure conditions.
- Despite large uncertainty, LFS data from OPF experiments is still useful to validate and optimize chemical mechanisms when the uncertainty in LFS measured from experiments is lower than that of chemical models, e.g., under high pressure and/or temperature conditions.

Declaration of Competing Interest

The authors declare that they have no conflicts of interest to this work.

Acknowledgments

The work was supported by National Natural Science Foundation of China (Nos. 51861135309 and 91741126). We thank Dr. Mike Kuznetsov for providing us the experimental data in [91].

References

[1] Lieuwen T, Yang V, Yetter R. Synthesis gas combustion: fundamentals and applications. CRC Press; 2009.
[2] Tartakovsky L, Sheintuch M. Fuel reforming in internal combustion engines. Prog Energy Combust 2018;67:88–114.
[3] Kalghatgi GT. The outlook for fuels for internal combustion engines. Int J Engine Res 2014;15(4):383–98.
[4] Fayaz H, Saidur R, Razali N, Anuar FS, Saleman AR, Islam MR. An overview of hydrogen as a vehicle fuel. Renew Sustain Energy Rev 2012;16(8):5511–28.
[5] Tang C, Zhang Y, Huang Z. Progress in combustion investigations of hydrogen enriched hydrocarbons. Renew Sustain Energy Rev 2014;30:195–216.
[6] Chintala V, Subramanian KA. A comprehensive review on utilization of hydrogen in a compression ignition engine under dual fuel mode. Renew Sustain Energy Rev 2017;70:472–91.
[7] Mehra RK, Duan H, Juknelevičius R, Ma F, Li J. Progress in hydrogen enriched compressed natural gas (HCNG) internal combustion engines – a comprehensive review. Renew Sustain Energy Rev 2017;80:1458–98.
[8] Perpignan AAV, Rao AG, Roekaerts DJEM. Flameless combustion and its potential towards gas turbines. Prog Energy Combust 2018;69:28–62. doi:10.1016/j.pecs.2018.06.002. http://www.sciencedirect.com/science/article/pii/S0360128517301296.
[9] Bothien MR, Ciani A, Wood JP, Fruechtel G. Toward decarbonized power generation with gas turbines by using sequential combustion for burning hydrogen. J Eng Gas Turbines Power 2019;141(12).
[10] Boloy RAM, Silveira JL, Tuna CE, Coronado CR, Antunes JS. Ecological impacts from syngas burning in internal combustion engine: technical and economic aspects. Renew Sustain Energy Rev 2011;15(9):5194–201.
[11] Sánchez AL, Williams FA. Recent advances in understanding of flammability characteristics of hydrogen. Prog Energy Combust 2014;41:1–55.
[12] Liu Z, Kong W, Consalvi J-L, Han W. H2/CO/air premixed and partially premixed flame structure at different pressures based on reaction limit analysis. Sci Bull 2018;63(19):1260–6.
[13] Zhao Z, Chen Z, Chen S. Correlations for the ignition delay times of hydrogen/air mixtures. Sci Bull 2011;56(2):215–21. doi:10.1007/s11434-010-4345-3.
[14] Park O, Veloo PS, Burbano H, Egolfopoulos FN. Studies of premixed and non-premixed hydrogen flames. Combust Flame 2015;162(4):1078–94. doi:10.1016/j.combustflame.2014.09.027. http://www.sciencedirect.com/science/article/pii/S0010218014003083.
[15] Law CK. Combustion physics. Cambridge: Cambridge University Press; 2006.
[16] Konnov AA, Mohammad A, Kishore VR, Kim NI, Prathap C, Kumar S. A comprehensive review of measurements and data analysis of laminar burning velocities for various fuel + air mixtures. Prog Energy Combust 2018;68:197–267.
[17] Kuo KK. Principles of combustion. Hoboken, New Jersey: John Wiley and Sons Inc; 2005.
[18] Poinsot T, Veynante D. Theoretical and numerical combustion. Philadelphia: Edwards; 2005.
[19] Peters N. Turbulent combustion. Cambridge: Cambridge University Press; 2000.
[20] Pitsch H. Large-eddy simulation of turbulent combustion. Annu Rev Fluid Mech 2006;38:453–82.
[21] Egolfopoulos FN, Hansen N, Ju Y, Kohse-Höinghaus K, Law CK, Qi F. Advances and challenges in laminar flame experiments and implications for combustion chemistry. Prog Energy Combust 2014;43:36–67. doi:10.1016/j.pecs.2014.04.004. http://www.sciencedirect.com/science/article/pii/S0360128514000252.
[22] Law CK, Wu F, Egolfopoulos FN, Gururajan V, Wang H. On the rational interpretation of data on laminar flame speeds and ignition delay times. Combust Sci Technol 2015;187(1–2):27–36. doi:10.1080/00102202.2014.970686.
[23] Lee HC, Jiang LY, Mohamad AA. A review on the laminar flame speed and ignition delay time of syngas mixtures. Int J Hydrog Energy 2014;39(2):1105–21. doi:10.1016/j.ijhydene.2013.10.068. http://www.sciencedirect.com/science/article/pii/S036031991302541X.
[24] Xie Y, Wang X, Bi H, Yuan Y, Wang J, Huang Z, Lei B. A comprehensive review on laminar spherically premixed flame propagation of syngas. Fuel Process Technol 2018;181:97–114. doi:10.1016/j.fuproc.2018.09.016. http://www.sciencedirect.com/science/article/pii/S0378382018309974.
[25] Sheen DA, Wang H. The method of uncertainty quantification and minimization using polynomial chaos expansions. Combust Flame 2011;158(12):2358–74.
[26] You X, Russi T, Packard A, Frenklach M. Optimization of combustion kinetic models on a feasible set. Proc Combust Inst 2011;33(1):509–16.
[27] Faghih M, Chen Z. The constant-volume propagating spherical flame method for laminar flame speed measurement. Sci Bull 2016;61(16):1296–310. doi:10.1007/s11434-016-1143-6.
[28] Rallis CJ, Garforth AM. The determination of laminar burning velocity. Prog Energy Combust 1980;6(4):303–29. doi:10.1016/0360-1285(80)90008-8. http://www.sciencedirect.com/science/article/pii/0360128580900088.
[29] Chen Z. On the accuracy of laminar flame speeds measured from outwardly propagating spherical flames: methane/air at normal temperature and pressure.

Combust Flame 2015;162(6):2442–53. doi:10.1016/j.combustflame.2015.02.012. h http://www.sciencedirect.com/science/article/pii/S0010218015000541.
[30] Tseng L-K, Ismail MA, Faeth GM. Laminar burning velocities and markstein numbers of hydrocarbonair flames. Combust Flame 1993;95(4):410–26. doi:10.1016/0010-2180(93)90007-P. http://www.sciencedirect.com/science/article/pii/001021809390007P.
[31] Gu XJ, Haq MZ, Lawes M, Woolley R. Laminar burning velocity and markstein lengths of methane-air mixtures. Combust Flame 2000;121(1):41–58. doi:10.1016/S0010-2180(99)00142-X. http://www.sciencedirect.com/science/article/pii/S001021809900142X.
[32] Rozenchan G, Zhu DL, Law CK, Tse SD. Outward propagation, burning velocities, and chemical effects of methane flames up to 60 ATM. Proc Combust Inst 2002;29(2):1461–70. doi:10.1016/S1540-7489(02)80179-1. http://www.sciencedirect.com/science/article/pii/S1540748902801791.
[33] Qin X, Ju Y. Measurements of burning velocities of dimethyl ether and air premixed flames at elevated pressures. Proc Combust Inst 2005;30(1):233–40. doi:10.1016/j.proci.2004.08.251. http://www.sciencedirect.com/science/article/pii/S0082078404003030.
[34] Lowry W, de Vries J, Krejci M, Petersen E, Serinyel Z, Metcalfe W, Curran H, Bourque G. Laminar flame speed measurements and modeling of pure alkanes and alkane blends at elevated pressures. J Eng Gas Turbine Power 2011;133(9). doi:10.1115/1.4002809. 091501.
[35] Nativel D, Pelucchi M, Frassoldati A, Comandini A, Cuoci A, Ranzi E, Chaumeix N, Faravelli T. Laminar flame speeds of pentanol isomers: an experimental and modeling study. Combust Flame 2016;166:1–18. doi:10.1016/j.combustflame.2015.11.012. http://www.sciencedirect.com/science/article/pii/S0010218015004034.
[36] Chen Z, Qin X, Ju Y, Zhao Z, Chaos M, Dryer FL. High temperature ignition and combustion enhancement by dimethyl ether addition to methane–air mixtures. Proc Combust Inst 2007;31(1):1215–22. doi:10.1016/j.proci.2006.07.177. http://www.sciencedirect.com/science/article/pii/S1540748906001908.
[37] Metghalchi M, Keck JC. Laminar burning velocity of propane-air mixtures at high temperature and pressure. Combust Flame 1980;38:143–54. doi:10.1016/0010-2180(80)90046-2. http://www.sciencedirect.com/science/article/pii/0010218080900462.
[38] Saeed K, Stone CR. Measurements of the laminar burning velocity for mixtures of methanol and air from a constant-volume vessel using a multizone model. Combust Flame 2004;139(1):152–66. doi:10.1016/j.combustflame.2004.08.008. http://www.sciencedirect.com/science/article/pii/S0010218004001610.
[39] Dahoe AE. Laminar burning velocities of hydrogen–air mixtures from closed vessel gas explosions. J Loss Prev Process Ind 2005;18(3):152–66. doi:10.1016/j.jlp.2005.03.007. http://www.sciencedirect.com/science/article/pii/S0950423005000392.
[40] Eisazadeh-Far K, Moghaddas A, Al-Mulki J, Metghalchi H. Laminar burning speeds of ethanol/air/diluent mixtures. Proc Combust Inst 2011;33(1):1021–7. doi:10.1016/j.proci.2010.05.105. http://www.sciencedirect.com/science/article/pii/S1540748910002683.
[41] Mitu M, Razus D, Giurcan V, Oancea D. Normal burning velocity and propagation speed of ethane–air: pressure and temperature dependence. Fuel 2015;147:27–34. doi:10.1016/j.fuel.2015.01.026. http://www.sciencedirect.com/science/article/pii/S001623611500040X.
[42] Askari O, Moghaddas A, Alholm A, Vien K, Alhazmi B, Metghalchi H. Laminar burning speed measurement and flame instability study of h2/CO/air mixtures at high temperatures and pressures using a novel multi-shell model. Combust Flame 2016;168:20–31. doi:10.1016/j.combustflame.2016.03.018. http://www.sciencedirect.com/science/article/pii/S0010218016300359.
[43] Omari A, Tartakovsky L. Measurement of the laminar burning velocityusing the confined and unconfined spherical flame methods – a comparative analysis. Combust Flame 2016;168:127–37. doi:10.1016/j.combustflame.2016.03.012. http://www.sciencedirect.com/science/article/pii/S0010218016300207.
[44] Halter F, Chen Z, Dayma G, Bariki C, Wang Y, Dagaut P, Chauveau C. Development of an optically accessible apparatus to characterize the evolution of spherically expanding flames under constant volume conditions. Combust Flame 2020;212:165–76.
[45] Clavin P. Dynamic behavior of premixed flame fronts in laminar and turbulent flows. Prog Energy Combust 1985;11(1):1–59. doi:10.1016/0360-1285(85)90012-7. http://www.sciencedirect.com/science/article/pii/0360128585900127.
[46] Balusamy S, Cessou A, Lecordier B. Direct measurement of local instantaneous laminar burning velocity by a new PIV algorithm. Exp Fluids 2011;50(4):1109–21. doi:10.1007/s00348-010-1027-5.
[47] Varea E, Modica V, Vandel A, Renou B. Measurement of laminar burning velocity and markstein length relative to fresh gases using a new postprocessing procedure: Application to laminar spherical flames for methane, ethanol and isooctane/air mixtures. Combust Flame 2012;159(2):577–90. doi:10.1016/j.combustflame.2011.09.002. http://www.sciencedirect.com/science/article/pii/S001021801100277X.
[48] Varea E, Modica V, Renou B, Boukhalfa AM. Pressure effects on laminar burning velocities and markstein lengths for isooctane–ethanol–air mixtures. Proc Combust Inst 2013;34(1):735–44. doi:10.1016/j.proci.2012.06.072. http://www.sciencedirect.com/science/article/pii/S1540748912001800.
[49] Giannakopoulos GK, Gatzoulis A, Frouzakis CE, Matalon M, Tomboulides AG. Consistent definitions of “flame displacement speed” and “markstein length” for premixed flame propagation. Combust Flame 2015;162(4):1249–64. doi:10.1016/j.combustflame.2014.10.015. http://www.sciencedirect.com/science/article/pii/S0010218014003368.
[50] Kelley AP, Law CK. Nonlinear effects in the extraction of laminar flame speeds from expanding spherical flames. Combust Flame 2009;156(9):1844–51. doi:10.1016/j.combustflame.2009.04.004. http://www.sciencedirect.com/science/article/pii/S001021800900114X.
[51] Halter F, Tahtouh T, Mounaïm-Rousselle C. Nonlinear effects of stretch on the flame front propagation. Combust Flame 2010;157(10):1825–32. doi:10.1016/j.combustflame.2010.05.013. http://www.sciencedirect.com/science/article/pii/S0010218010001550.
[52] Chen Z. On the extraction of laminar flame speed and markstein length from outwardly propagating spherical flames. Combust Flame 2011;158(2):291–300. doi:10.1016/j.combustflame.2010.09.001. http://www.sciencedirect.com/science/article/pii/S0010218010002440.
[53] Chen Z, Burke MP, Ju Y. Effects of lewis number and ignition energy on the determination of laminar flame speed using propagating spherical flames. Proc Combust Inst 2009;32(1):1253–60. doi:10.1016/j.proci.2008.05.060. http://www.sciencedirect.com/science/article/pii/S154074890800285X.
[54] Chen Z. Effects of radiation and compression on propagating spherical flames of methane/air mixtures near the lean flammability limit. Combust Flame 2010;157(12):2267–76. doi:10.1016/j.combustflame.2010.07.010. http://www.sciencedirect.com/science/article/pii/S0010218010001987.
[55] Dai P, Chen Z. Supersonic reaction front propagation initiated by a hot spot in n-heptane/air mixture with multistage ignition. Combust Flame 2015;162(11):4183–93. doi:10.1016/j.combustflame.2015.08.002. http://www.sciencedirect.com/science/article/pii/S0010218015002588.
[56] Jayachandran J, Zhao R, Egolfopoulos FN. Determination of laminar flame speeds using stagnation and spherically expanding flames: Molecular transport and radiation effects. Combust Flame 2014;161(9):2305–16. doi:10.1016/j.combustflame.2014.03.009. http://www.sciencedirect.com/science/article/pii/S0010218014000893.
[57] Xiouris C, Ye T, Jayachandran J, Egolfopoulos FN. Laminar flame speeds under engine-relevant conditions: Uncertainty quantification and minimization in spherically expanding flame experiments. Combust Flame 2016;163:270–83. doi:10.1016/j.combustflame.2015.10.003. http://www.sciencedirect.com/science/article/pii/S0010218015003508.
[58] Strang G. On the construction and comparison of difference schemes. SIAM J Numer Anal 1968;5(3):506–17. doi:10.1137/0705041.
[59] Chen Z. Effects of hydrogen addition on the propagation of spherical methane/air flames: a computational study. Int J Hydrog Energy 2009;34(15):6558–67. doi:10.1016/j.ijhydene.2009.06.001. http://www.sciencedirect.com/science/article/pii/S0360319909008672.
[60] Qi C, Dai P, Yu H, Chen Z. Different modes of reaction front propagation in n-heptane/air mixture with concentration non-uniformity. Proc Combust Inst 2017;36(3):3633–41. doi:10.1016/j.proci.2016.06.086. http://www.sciencedirect.com/science/article/pii/S1540748916301444.
[61] Dai P, Chen Z, Chen S, Ju Y. Numerical experiments on reaction front propagation in n-heptane/air mixture with temperature gradient. Proc Combust Inst 2015;35(3):3045–52. doi:10.1016/j.proci.2014.06.102. http://www.sciencedirect.com/science/article/pii/S1540748914002600.
[62] Dai P, Qi C, Chen Z. Effects of initial temperature on autoignition and detonation development in dimethyl ether/air mixtures with temperature gradient. Proc Combust Inst 2017;36(3):3643–50. doi:10.1016/j.proci.2016.08.014. http://www.sciencedirect.com/science/article/pii/S1540748916304035.
[63] Yu H, Chen Z. End-gas autoignition and detonation development in a closed chamber. Combust Flame 2015;162(11):4102–11. doi:10.1016/j.combustflame.2015.08.018. http://www.sciencedirect.com/science/article/pii/S0010218015002850.
[64] Zhang W, Gou X, Chen Z. Effects of water vapor dilution on the minimum ignition energy of methane, n-butane and n-decane at normal and reduced pressures. Fuel 2017;187:111–16. doi:10.1016/j.fuel.2016.09.057. http://www.sciencedirect.com/science/article/pii/S0016236116309140.
[65] Yu H, Qi C, Chen Z. Effects of flame propagation speed and chamber size on end-gas autoignition. Proc Combust Inst 2017;36(3):3533–41. doi:10.1016/j.proci.2016.07.123. http://www.sciencedirect.com/science/article/pii/S1540748916303819.
[66] Zhang W, Faqih M, Gou X, Chen Z. Numerical study on the transient evolution of a premixed cool flame. Combust Flame 2018;187:129–36. doi:10.1016/j.combustflame.2017.09.009. http://www.sciencedirect.com/science/article/pii/S0010218017303395.
[67] Faghih M, Chen Z. Two-stage heat release in nitromethane/air flame and its impact on laminar flame speed measurement. Combust Flame 2017;183:157–65. doi:10.1016/j.combustflame.2017.05.013. http://www.sciencedirect.com/science/article/pii/S0010218017301803.
[68] Faghih M, Gou X, Chen Z. The explosion characteristics of methane, hydrogen and their mixtures: a computational study. J Loss Prev Process Ind 2016;40:131–8. doi:10.1016/j.jlp.2015.12.015. http://www.sciencedirect.com/science/article/pii/S0950423015300930.
[69] Kee RJ, Rupley FM, Miller JA. Chemkin-ii: a fortran package for the analysis of gas-phase chemical kinetics. Sand Natl Lab Rep 1989;SAND89-8009B.
[70] Sun M, Takayama K. Conservative smoothing on an adaptive quadrilateral grid. J Comput Phys 1999;150(1):143–80. doi:10.1006/jcph.1998.6167. http://www.sciencedirect.com/science/article/pii/S0021999198961678.
[71] Chen S, Xu K, Lee C, Cai Q. A unified gas kinetic scheme with moving mesh and velocity space adaptation. J Comput Phys 2012;231(20):6643–64. doi:10.1016/j.jcp.2012.05.019. http://www.sciencedirect.com/science/article/pii/S0021999112002616.
[72] Wang Y, Han W, Chen Z. Effects of fuel stratification on ignition kernel development and minimum ignition energy of n-decane/air mixtures. Proc Combust Inst 2019;37(2):1623–30.
[73] Li J, Zhao Z, Kazakov A, Dryer FL, et al. An updated comprehensive kinetic model

of hydrogen combustion. Int J Chem Kinet 2004;36(10):566–75. doi:10.1002/kin.20026. https://onlinelibrary.wiley.com/doi/abs/10.1002/kin.20026.

[74] Davis SG, Joshi AV, Wang H, Egolfopoulos F. An optimized kinetic model of H2/CO combustion. Proc Combust Inst 2005;30(1):1283–92. doi:10.1016/j.proci.2004.08.252. http://www.sciencedirect.com/science/article/pii/S0082078404003054.

[75] Bongers H, De Goey LPH. The effect of simplified transport modeling on the burning velocity of laminar premixed flames. Combust Sci Technol 2003;175(10):1915–28. doi:10.1080/713713111.

[76] Yang F, Law CK, Sung CJ, Zhang HQ. A mechanistic study of soret diffusion in hydrogen-air flames. Combust Flame 2010;157(1):192–200. doi:10.1016/j.combustflame.2009.09.018. http://www.sciencedirect.com/science/article/pii/S0010218009002764.

[77] Liang W, Chen Z, Yang F, Zhang H. Effects of soret diffusion on the laminar flame speed and markstein length of syngas/air mixtures. Proc Combust Inst 2013;34(1):695–702. doi:10.1016/j.proci.2012.06.048. http://www.sciencedirect.com/science/article/pii/S1540748912001563.

[78] Faghih M, Han W, Chen Z. Effects of soret diffusion on premixed flame propagation under engine-relevant conditions. Combust Flame 2018;194:175–9. doi:10.1016/j.combustflame.2018.04.031. http://www.sciencedirect.com/science/article/pii/S0010218018301895.

[79] Liang W, Law CK, Chen Z. Ignition of hydrogen/air mixtures by a heated kernel: role of soret diffusion. Combust Flame 2018;197:416–22. doi:10.1016/j.combustflame.2018.08.015. http://www.sciencedirect.com/science/article/pii/S0010218018303808.

[80] Taylor SC. Burning velocity and the influence of flame stretch. University of Leeds; 1991.

[81] Aung KT, Hassan MI, Faeth GM. Flame stretch interactions of laminar premixed hydrogen/air flames at normal temperature and pressure. Combust Flame 1997;109(1):1–24. doi:10.1016/S0010-2180(96)00151-4. http://www.sciencedirect.com/science/article/pii/S0010218096001514.

[82] Tse SD, Zhu DL, Law CK. Morphology and burning rates of expanding spherical flames in H2/O2/inert mixtures up to 60 atmospheres. Proc Combust Inst 2000;28(2):1793–800. doi:10.1016/S0082-0784(00)80581-0. http://www.sciencedirect.com/science/article/pii/S0082078400805810.

[83] Kwon OC, Faeth GM. Flame/stretch interactions of premixed hydrogen-fueled flames: measurements and predictions. Combust Flame 2001;124(4):590–610. doi:10.1016/S0010-2180(00)00229-7. http://www.sciencedirect.com/science/article/pii/S0010218000002297.

[84] Lamoureux N, Djebaili-Chaumeix N, Paillard CE. Laminar flame velocity determination for H2-air-He-CO2 mixtures using the spherical bomb method. Exp Therm Fluid Sci 2003;27(4):385–93. doi:10.1016/S0894-1777(02)00243-1. Second Mediterranean Combustion Symposium.

[85] Verhelst S, Woolley R, Lawes M, Sierens R. Laminar and unstable burning velocities and markstein lengths of hydrogen–air mixtures at engine-like conditions. Proc Combust Inst 2005;30(1):209–16. doi:10.1016/j.proci.2004.07.042. http://www.sciencedirect.com/science/article/pii/S0082078404000402.

[86] Huang Z, Zhang Y, Zeng K, Liu B, Wang Q, Jiang D. Measurements of laminar burning velocities for natural gas–hydrogen–air mixtures. Combust Flame 2006;146(1):302–11. doi:10.1016/j.combustflame.2006.03.003. http://www.sciencedirect.com/science/article/pii/S0010218006000873.

[87] Bradley D, Lawes M, Liu K, Verhelst S, Woolley R. Laminar burning velocities of lean hydrogen–air mixtures at pressures up to 1.0 MPa. Combust Flame 2007;149(1):162–72. doi:10.1016/j.combustflame.2006.12.002. http://www.sciencedirect.com/science/article/pii/S0010218006002811.

[88] Tang C, Huang Z, Jin C, He J, Wang J, Wang X, Miao H. Laminar burning velocities and combustion characteristics of propane–hydrogen–air premixed flames. Int J Hydrog Energy 2008;33(18):4906–14. doi:10.1016/j.ijhydene.2008.06.063. http://www.sciencedirect.com/science/article/pii/S0360319908007702.

[89] Hu E, Huang Z, He J, Jin C, Zheng J. Experimental and numerical study on laminar burning characteristics of premixed methane–hydrogen–air flames. Int J Hydrog Energy 2009;34(11):4876–88. doi:10.1016/j.ijhydene.2009.03.058. 2nd International Workshop on Hydrogen.

[90] Burke MP, Chen Z, Ju Y, Dryer FL. Effect of cylindrical confinement on the determination of laminar flame speeds using outwardly propagating flames. Combust Flame 2009;156(4):771–9. doi:10.1016/j.combustflame.2009.01.013. http://www.sciencedirect.com/science/article/pii/S0010218009000200.

[91] Kuznetsov M, Kobelt S, Grune J, Jordan T. Flammability limits and laminar flame speed of hydrogen–air mixtures at sub-atmospheric pressures. Int J Hydrog Energy 2012;37(22):17580–8. doi:10.1016/j.ijhydene.2012.05.049. http://www.sciencedirect.com/science/article/pii/S0360319912011925.

[92] Krejci MC, Mathieu O, Vissotski AJ, Ravi S, Sikes TG, Petersen EL, Kérmonès A, Metcalfe W, Curran HJ. Laminar flame speed and ignition delay time data for the kinetic modeling of hydrogen and syngas fuel blends. J Eng Gas Turbine Power 2013;135(2). doi:10.1115/1.4007737. 021503; https://asmedigitalcollection.asme.org/gasturbinespower/article-pdf/135/2/021503/6156105/gtp_135_2_021503.pdf.

[93] Dayma G, Halter F, Dagaut P. New insights into the peculiar behavior of laminar burning velocities of hydrogen–air flames according to pressure and equivalence ratio. Combust Flame 2014;161(9):2235–41. doi:10.1016/j.combustflame.2014.02.009. http://www.sciencedirect.com/science/article/pii/S0010218014000686.

[94] Beeckmann J, Pitsch H. Laminar burning velocities of spherically expanding hydrogen/air mixtures for temperatures up to 423 k at ambient pressure. In: Proceedings of the Twenty-sixth International Colloquium on the Dynamics of Explosions and Reactive Systems; 2017. p. Paper1175.

[95] Grosseuvres R, Comandini A, Bentaib A, Chaumeix N, et al. Combustion properties of H2/N2/O2/steam mixtures. Proc Combust Inst 2019;37(2):1537–46.

[96] McLean IC, Smith DB, Taylor SC. The use of carbon monoxide/hydrogen burning velocities to examine the rate of the CO + OH reaction. Proc Combust Inst 1994;25(1):749–57. doi:10.1016/S0082-0784(06)80707-1. Twenty-Fifth Symposium (International) on Combustion; http://www.sciencedirect.com/science/article/pii/S0082078406807071.

[97] Hassan MI, Aung KT, Faeth GM. Properties of laminar premixed CO/H/Air flames at various pressures. J Propuls Power 1997;13(2):239–45. doi:10.2514/2.5154.

[98] Sun H, Yang SI, Jomaas G, Law CK. High-pressure laminar flame speeds and kinetic modeling of carbon monoxide/hydrogen combustion. Proc Combust Inst 2007;31(1):439–46. doi:10.1016/j.proci.2006.07.193. http://www.sciencedirect.com/science/article/pii/S1540748906002045.

[99] Prathap C, Ray A, Ravi MR. Investigation of nitrogen dilution effects on the laminar burning velocity and flame stability of syngas fuel at atmospheric condition. Combust Flame 2008;155(1):145–60. doi:10.1016/j.combustflame.2008.04.005. http://www.sciencedirect.com/science/article/pii/S0010218008001016.

[100] Bouvet N, Chauveau C, Gökalp I, Halter F. Experimental studies of the fundamental flame speeds of syngas (H2/CO)/air mixtures. Proc Combust Inst 2011;33(1):913–20. doi:10.1016/j.proci.2010.05.088. http://www.sciencedirect.com/science/article/pii/S1540748910002075.

[101] Singh D, Nishiie T, Tanvir S, Qiao L. An experimental and kinetic study of syngas/air combustion at elevated temperatures and the effect of water addition. Fuel 2012;94:448–56. doi:10.1016/j.fuel.2011.11.058. http://www.sciencedirect.com/science/article/pii/S0016236111007538.

[102] Ai Y, Zhou Z, Chen Z, Kong W. Laminar flame speed and markstein length of syngas at normal and elevated pressures and temperatures. Fuel 2014;137:339–45. doi:10.1016/j.fuel.2014.08.004. http://www.sciencedirect.com/science/article/pii/S001623611400773X.

[103] Li H-M, Li G-X, Sun Z-Y, Zhai Y, Zhou Z-H. Measurement of the laminar burning velocities and markstein lengths of lean and stoichiometric syngas premixed flames under various hydrogen fractions. Int J Hydrog Energy 2014;39(30):17371–80. doi:10.1016/j.ijhydene.2014.07.177. http://www.sciencedirect.com/science/article/pii/S0360319914023271.

[104] Gong X, Huo J, Ren Z, Law CK. Extrapolation and DNS-mapping in determining laminar flame speeds of syngas/air mixtures. Combust Flame 2019;200:365–73.

[105] Kee RJ, Grcar JF, Smooke MD, Miller JA. A fortran program for modeling steady laminar one-dimensional premixed flames. Sand Natl Lab Rep 1985;SAND85-8240.

[106] Santner J, Haas FM, Dryer FL, Ju Y. High temperature oxidation of formaldehyde and formyl radical: a study of 1,3,5-trioxane laminar burning velocities. Proc Combust Inst 2015;35(1):687–94. doi:10.1016/j.proci.2014.05.014. http://www.sciencedirect.com/science/article/pii/S1540748914000170.

[107] Beeckmann J, Chaumeix N, Dagaut P, Dayma G, Egolfopoulos FN, Foucher F, De Goey LPH, Halter F, Konnov AA, Mounaïm-Rousselle C, Pitsch H, Renou B, varea E, Volkov E. Collaborative study for accurate measurements of laminar burning velocity. In: Proceedings of the European Combustion Meeting; 2013. p. P3–76. Lund, Sweden.

[108] Zhang Z, Cheng P, Tan J, Liang J, Li Y, Li G. The uncertainty of laminar burning velocity of premixed H2-air flame induced by the non-uniform initial temperature field inside the constant-volume combustion vessel. Int J Hydrog Energy 2018;43(45):21049–59. doi:10.1016/j.ijhydene.2018.09.037. http://www.sciencedirect.com/science/article/pii/S0360319918328830.

[109] Bradley D, Gaskell PH, Gu XJ. Burning velocities, markstein lengths, and flame quenching for spherical methane-air flames: A computational study. Combust Flame 1996;104(1):176–98. doi:10.1016/0010-2180(95)00115-8. http://www.sciencedirect.com/science/article/pii/0010218095001158.

[110] Kim HH, Won SH, Santner J, Chen Z, Ju Y. Measurements of the critical initiation radius and unsteady propagation of n-decane/air premixed flames. Proc Combust Inst 2013;34(1):929–36. doi:10.1016/j.proci.2012.07.035. http://www.sciencedirect.com/science/article/pii/S1540748912003276.

[111] Zhou M, Li G, Zhang Z, Liang J, Tian L. Effect of ignition energy on the initial propagation of ethanol/air laminar premixed flames: An experimental study. Energy Fuels 2017;31(9):10023–31. doi:10.1021/acs.energyfuels.7b00965.

[112] Santner JS, Won SH, Ju Y. Chemistry and transport effects on critical flame initiation radius for alkanes and aromatic fuels. Proc Combust Inst 2017;36(1):1457–65. doi:10.1016/j.proci.2016.05.014. http://www.sciencedirect.com/science/article/pii/S1540748916300141.

[113] Cai X, Wang J, Zhao H, Xie Y, Huang Z. Effects of initiation radius selection and lewis number on extraction of laminar burning velocities from spherically expanding flames. Combust Sci Technol 2018;190(2):286–311. doi:10.1080/00102202.2017.1389912.

[114] Chen Z, Burke MP, Ju Y. Effects of compression and stretch on the determination of laminar flame speeds using propagating spherical flames. Combust Theory Model 2009;13(2):343–64. doi:10.1080/13647830802632192.

[115] Chen Z. Effects of radiation and compression on propagating spherical flames of methane/air mixtures near the lean flammability limit. Combust Flame 2010;157(12):2267–76. doi:10.1016/j.combustflame.2010.07.010. http://www.sciencedirect.com/science/article/pii/S0010218010001987.

[116] Bonhomme A, Selle L, Poinsot T. Curvature and confinement effects for flame speed measurements in laminar spherical and cylindrical flames. Combust Flame 2013;160(7):1208–14. doi:10.1016/j.combustflame.2013.02.003. http://www.sciencedirect.com/science/article/pii/S001021801300045X.

[117] Jomaas G, Law CK, Bechtold JK. On transition to cellularity in expanding spherical flames. J Fluid Mech 2007;583:1–26. doi:10.1017/S0022112007005885.

[118] Vu TM, Park J, Kwon OB, Kim JS. Effects of hydrocarbon addition on cellular instabilities in expanding syngas–air spherical premixed flames. Int J Hydrog Energy 2009;34(16):6961–9. doi:10.1016/j.ijhydene.2009.06.067. 4th Dubrovnik Conference; http://www.sciencedirect.com/science/article/pii/S0360319909009689.

[119] Vu TM, Park J, Kim JS, Kwon OB, Yun JH, Keel SI, et al. Experimental study on cellular instabilities in hydrocarbon/hydrogen/carbon monoxide–air premixed flames. Int J Hydrog Energy 2011;36(11):6914–24. doi:10.1016/j.ijhydene.2011.02.085. http://www.sciencedirect.com/science/article/pii/S0360319911004393.

[120] Cai X, Wang J, Zhao H, Zhang M, Huang Z. Flame morphology and self-acceleration of syngas spherically expanding flames. Int J Hydrog Energy 2018;43(36):17531–41. doi:10.1016/j.ijhydene.2018.07.140. http://www.sciencedirect.com/science/article/pii/S0360319918323644.

[121] Chen Z, Qin X, Xu B, Ju Y, Liu F. Studies of radiation absorption on flame speed and flammability limit of CO2 diluted methane flames at elevated pressures. Proc Combust Inst 2007;31(2):2693–700. doi:10.1016/j.proci.2006.07.202. http://www.sciencedirect.com/science/article/pii/S1540748906002185.

[122] Santner J, Haas FM, Ju Y, Dryer FL, et al. Uncertainties in interpretation of high pressure spherical flame propagation rates due to thermal radiation. Combust Flame 2014;161(1):147–53. doi:10.1016/j.combustflame.2013.08.008. http://www.sciencedirect.com/science/article/pii/S0010218013003027.

[123] Yu H, Han W, Santner J, Gou X, Sohn CH, Ju Y, Chen Z. Radiation-induced uncertainty in laminar flame speed measured from propagating spherical flames. Combust Flame 2014;161(11):2815–24. doi:10.1016/j.combustflame.2014.05.012. http://www.sciencedirect.com/science/article/pii/S0010218014001424.

[124] Chen Z, Gou X, Ju Y. Studies on the outwardly and inwardly propagating spherical flames with radiative loss. Combust Sci Technol 2010;182(2):124–42. doi:10.1080/00102200903299850.

[125] Zhang H, Guo P, Chen Z. Outwardly propagating spherical flames with thermally sensitive intermediate kinetics and radiative loss. Combust Sci Technol 2013;185(2):226–48. doi:10.1080/00102202.2012.715607.

[126] Sohn CH, Chen Z, Ju Y. Effects of radiation on the uncertainty of flame speed determination using spherically propagating flames with CO/CO2/H2O dilutions at elevated pressures. Int J Heat Mass Transf 2015;86:820–5. doi:10.1016/j.ijheatmasstransfer.2015.03.062. http://www.sciencedirect.com/science/article/pii/S0017931015003282.

[127] Chen Z. Effects of radiation on large-scale spherical flame propagation. Combust Flame 2017;183:66–74. doi:10.1016/j.combustflame.2017.04.031. http://www.sciencedirect.com/science/article/pii/S0010218017301669.

[128] Chen Z. Effects of radiation absorption on spherical flame propagation and radiation-induced uncertainty in laminar flame speed measurement. Proc Combust Inst 2017;36(1):1129–36. doi:10.1016/j.proci.2016.05.003. http://www.sciencedirect.com/science/article/pii/S1540748916300037.

[129] Qiao L, Gu Y, Dahm WJA, Oran ES, Faeth GM. Near-limit laminar burning velocities of microgravity premixed hydrogen flames with chemically-passive fire suppressants. Proc Combust Inst 2007;31(2):2701–9. doi:10.1016/j.proci.2006.07.012. http://www.sciencedirect.com/science/article/pii/S1540748906000150.

[130] Qiao L, Gu Y, Dahm WJA, Oran ES, Faeth GM. A study of the effects of diluents on near-limit h2–air flames in microgravity at normal and reduced pressures. Combust Flame 2007;151(1):196–208. doi:10.1016/j.combustflame.2007.06.013. http://www.sciencedirect.com/science/article/pii/S0010218007001563.

[131] Qiao L, Gan Y, Nishiie T, Dahm WJA, Oran ES. Extinction of premixed methane/air flames in microgravity by diluents: Effects of radiation and lewis number. Combust Flame 2010;157(8):1446–55. doi:10.1016/j.combustflame.2010.04.004. http://www.sciencedirect.com/science/article/pii/S0010218010001082.

[132] Wang S-F, Zhang H, Jarosinski J, Gorczakowski A, Podfilipski J. Laminar burning velocities and markstein lengths of premixed methane/air flames near the lean flammability limit in microgravity. Combust Flame 2010;157(4):667–75. doi:10.1016/j.combustflame.2010.01.006. http://www.sciencedirect.com/science/article/pii/S0010218010000179.

[133] Sun Z-Y, Li G-X, Li H-M, Zhai Y, Zhou Z-H. Buoyant unstable behavior of initially spherical lean hydrogen-air premixed flames. Energies 2014;7(8):4938–56. doi:10.3390/en7084938. https://www.mdpi.com/1996-1073/7/8/4938.

[134] Kelley AP, Bechtold JK, Law CK. Premixed flame propagation in a confining vessel with weak pressure rise. J Fluid Mech 2012;691:26–51.

[135] Wu F, Liang W, Chen Z, Ju Y, Law CK. Uncertainty in stretch extrapolation of laminar flame speed from expanding spherical flames. Proc Combust Inst 2015;35(1):663–70. doi:10.1016/j.proci.2014.05.065. http://www.sciencedirect.com/science/article/pii/S1540748914000686.

[136] Varea E, Beeckmann J, Pitsch H, Chen Z, Renou B. Determination of burning velocities from spherically expanding h2/air flames. Proc Combust Inst 2015;35(1):711–19. doi:10.1016/j.proci.2014.05.137. http://www.sciencedirect.com/science/article/pii/S1540748914001400.

[137] Liang W, Wu F, Law CK. Extrapolation of laminar flame speeds from stretched flames: Role of finite flame thickness. Proc Combust Inst 2017;36(1):1137–43. doi:10.1016/j.proci.2016.08.074. http://www.sciencedirect.com/science/article/pii/S1540748916304631.

[138] Li X, Hu E, Meng X, Peng C, Lu X, Huang Z. Effect of lewis number on nonlinear extrapolation methods from expanding spherical flames. Combust Sci Technol 2017;189(9):1510–26. doi:10.1080/00102202.2017.1305369.

[139] Jayachandran J, Lefebvre A, Zhao R, Halter F, Varea E, Renou B, Egolfopoulos FN. A study of propagation of spherically expanding and counterflow laminar flames using direct measurements and numerical simulations. Proc Combust Inst 2015;35(1):695–702. doi:10.1016/j.proci.2014.05.031. http://www.sciencedirect.com/science/article/pii/S1540748914000340.

[140] Lipatnikov AN, Shy SS, Li W-y, et al. Experimental assessment of various methods of determination of laminar flame speed in experiments with expanding spherical flames with positive markstein lengths. Combust Flame 2015;162(7):2840–54. doi:10.1016/j.combustflame.2015.04.003. http://www.sciencedirect.com/science/article/pii/S0010218015001145

[141] Huo J, Yang S, Ren Z, Zhu D, Law CK. Uncertainty reduction in laminar flame speed extrapolation for expanding spherical flames. Combust Flame 2018;189:155–62. doi:10.1016/j.combustflame.2017.10.032. http://www.sciencedirect.com/science/article/pii/S0010218017304297

[142] Chen Z, Ju Y. Theoretical analysis of the evolution from ignition kernel to flame ball and planar flame. Combust Theory Model 2007;11(3):427–53. doi:10.1080/13647830600999850.

[143] Kelley AP, Jomaas G, Law CK. Critical radius for sustained propagation of spark-ignited spherical flames. Combust Flame 2009;156(5):1006–13. doi:10.1016/j.combustflame.2008.12.005. http://www.sciencedirect.com/science/article/pii/S0010218008003933

[144] Chen Z, Burke MP, Ju Y. On the critical flame radius and minimum ignition energy for spherical flame initiation. Proc Combust Inst 2011;33(1):1219–26. doi:10.1016/j.proci.2010.05.005. http://www.sciencedirect.com/science/article/pii/S1540748910000180

[145] Zhang W, Chen Z, Kong W. Effects of diluents on the ignition of premixed H2/air mixtures. Combust Flame 2012;159(1):151–60. doi:10.1016/j.combustflame.2011.05.017. http://www.sciencedirect.com/science/article/pii/S0010218011001635

[146] Bradley D, Hicks RA, Lawes M, Sheppard CGW, Woolley R. The measurement of laminar burning velocities and markstein numbers for iso-octane–air and iso-octane–n-heptane–air mixtures at elevated temperatures and pressures in an explosion bomb. Combust Flame 1998;115(1):126–44. doi:10.1016/S0010-2180(97)00349-0. http://www.sciencedirect.com/science/article/pii/S0010218097003490

[147] Ronney PD, Wachman HY. Effect of gravity on laminar premixed gas combustion i: flammability limits and burning velocities. Combust Flame 1985;62(2):107–19. doi:10.1016/0010-2180(85)90139-7. http://www.sciencedirect.com/science/article/pii/0010218085901397

[148] Markstein GH. Experimental and theoretical studies of flame-front stability. In: Pelcé P, editor. Dynamics of curved fronts. San Diego: Academic Press; 1988. p. 413–23.

[149] Li X, Hu E, Meng X, Peng C, Lu X, Huang Z. Effect of lewis number on nonlinear extrapolation methods from expanding spherical flames. Combust Sci Technol 2017;189(9):1510–26.

[150] Qiao L, Kim CH, Faeth GM. Suppression effects of diluents on laminar premixed hydrogen/oxygen/nitrogen flames. Combust Flame 2005;143(1):79–96. doi:10.1016/j.combustflame.2005.05.004. http://www.sciencedirect.com/science/article/pii/S0010218005001343